Metal pollutants in Indian continental coastal marine sediment along a 3,700 km transect: An Electron Paramagnetic Resonance spectroscopic study

R. Alagarsamy[a], S.R. Hoon[b*]

a. CSIR-National Institute of Oceanography, Donapaula, Goa-403 004, India. e-mail: alagar@nio.org

b. School of Science & the Environment, Faculty of Science & Engineering, Manchester Metropolitan University, Manchester, M1 5GD, UK. e-mail: s.hoon@mmu.ac.uk

Corresponding author: s.hoon@mmu.ac.uk

Abstract

We report the analysis and geographical distribution of anthropogenically impacted marine surficial sediments along a 3,700 km transect around the continental shelf of India. Sediments have been studied using a mixed analytical approach; high sensitivity electron paramagnetic resonance (EPR), chemical analysis and environmental magnetism. Indian coastal marine deposits are heavily influenced by monsoon rains flushing sediment of geological and anthropogenic origin out of the subcontinental river systems. That is, climatic, hydro-, geo- and anthropogenic spheres couple strongly to determine the nature of Indian coastal sediments. Enrichment of Ni, Cu and Cr is observed in shelf sediments along both east and west coasts associated with industrialised activities in major urban areas. In the Gulf of Cambay and the Krishna and Visakhapatnam deltaic regions, levels of Ni and Cr pollutants (≥ 80 and ≥ 120 ppm respectively) are observed, sufficient to cause at least medium adverse biological effects in the marine ecosystem. In these areas sediment EPR spectra differ in characteristic from those of less impacted ones. Modelling enables deconvolution of EPR spectra. In conjunction with environmental magnetism techniques, EPR has been used to characterise species composition in coastal depositional environments. Paramagnetic species can be identified and their relative concentrations determined. EPR g-values provide information about the chemical and magnetic environment of metals. We observe g-values of up to 5.5 and large g-shifts indicative of the presences of a number of para and ferrimagnetic impurities in the sediments. EPR has enabled the characterisation of species composition in coastal depositional environments, yielding marine sediment environmental 'fingerprints'. The approach demonstrates the potential of EPR spectroscopy in the mapping and evaluation of the concentration and chemical speciation in paramagnetic metals in sediments from marine shelf environments and their potential for source apportionment and environmental impact assessment.

1 Introduction

Elevated levels of Co and Zn indicative of anthropogenic input have been observed in Indian rivers (Alagarsamy and Zhang 2005). Thus, it is unsurprising that metal enrichment of Co and Cu associated with industrial activities occurs in Indian continental shelf sediments along both east and west coasts proximal to major urban areas (Alagarsamy and Zhang, 2010). Indian coastal marine deposits are heavily influenced by monsoon rains flushing sediment out of the river systems, sediments both geological and anthropogenic in origin. That is climatic, hydro-, geo- and anthropogenic spheres couple strongly to determine the nature and biological impact of these sediments. Techniques commonly employed in the analysis and detection of trace metals in the marine environment include atomic absorption spectroscopy, emission spectroscopy and neutron activation. Whilst these techniques give qualitative and quantitative information, they do not yield information on the trace metal micro-environment. In contrast, the high sensitivity of electron paramagnetic resonance (EPR) spectroscopy, also known as electron spin resonance (ESR) spectroscopy, provides additional information on metallic oxidation states and the chemical environment of magnetically active minerals whether of geological or anthropogenic origin. That is, EPR has the capacity to yield quantitative and qualitative data that is complementary to that obtained from other bulk chemical and magnetic techniques. This is demonstrated here in a study of anthropogenically impacted Indian coastal marine sediments along a 3,700km transect.

EPR has been used to investigate the behaviour of paramagnetic particulate species in marine (Wakeman and Carpenter 1974, Crook et al. 2002,) and anoxic sediments (Billon et al. 2003), rivers (Boughriet et al. 1992), estuaries (Ouddane et al. 2001) and terrestrial (Küçükuysal et al. 2011) materials. Otamendi et al. (2006) have employed EPR to study the stratigraphy of geological marine sediments in southwestern Venezuela. EPR has also been used quantitatively to determine trace levels of Cu in seawater (Virmani and Zeller 1974) and to monitor low concentrations of Mn and other heavy metals in natural water systems (Angino et al. 1971). Sun et al. (2008) have proposed the use of EPR to detect organic free radicals and trivalent iron pollution in mangrove swamps. Heise (1968) investigated the variation of transition metal EPR spectra with sediment depth in marine sediments although without detailed analysis of sediment composition. Violante et al. (2010) have used EPR to complement other spectroscopic techniques in the identification of terrestrial metal complexes at the surfaces of Al, Fe and Mn oxides in silicate clays and soil organic matter. Espinosa et al. (2001) have employed EPR in the analysis of V(IV) porphyrins in petroleum products. Guedes et al. (2003) employed EPR in the

characterisation of the molecular structure of asphaltenes in Brazilian oil whilst multicomponent systems have been studied in the laboratory by Guilbault and Misel (1969, 1970), Guilbault and Moyer (1970). Mangrich et al. (2009) have used EPR to trace the provenances of dusts by studying sunlight bleaching of Ti E_1' electron trap centres in quartz which are induced by natural radiation (Gao et al. 2009). Nagashima et al. (2012) have used variation in the EPR signal intensity of E_1' centres to assess the contribution of detrital materials from the Yukon River to continental shelf sediments in the Bering Sea. Bahain et al. (2007) have used the EPR response of E_1' centres in quartz and carbonates to date archaeological deposits buried in river sediments and Tissoux et al. (2008) have used active E_1' centres to date Pleistocene deposits.

Although EPR has been applied to geochemical and terrestrial systems it has found more limited application to the analysis of marine systems. This is surprising as its detection limit is comparable to the techniques more commonly used for the chemical analysis of sediments. We believe that the present study is the first of its kind to apply EPR analysis combined with detailed modelling of para- and ferri-magnetic components to marine continental shelf sediments along the east and west coasts of India providing better understanding of the status of sediment pollution. Our integrated EPR, chemical and environmental magnetic methodology also enables the determination of a suite of parameters that yield a 'fingerprint' for these surficial coastal sediments with the potential to enable source apportionment.

2 Study area

2.1 Geographic and climatic setting

Geographically the subcontinent of India (Fig. 1) embraces tropical and subtropical climatic zones which are dominated by monsoon systems. These are characterised by strong seasonal variations alternating between warm-humid to cold-arid conditions resulting in wet and dry seasons alone and significant seasonal variation in rainfall and temperature. The gradient of these climatic zones is affected predominantly by the sharp altitudinal changes in the northern half of the subcontinent where the Himalaya form the major relief. The Himalaya act as a barrier to the cold northerly winds from Central Asia maintaining the pattern of the Indian Ocean monsoon circulation. The Thar Desert in the north west of India allows oceanic atmospheric circulation and promotes sediment dust-aerosol influx deep into the continent. The southwest monsoon is divided west and east of the Indian peninsular into the Arabian Sea and weaker Bay of Bengal branches, respectively. The latter results in regional turbulence due to the rapid altitudinal

4

differences and narrowing orography. The former branch moves northwards along the Western Ghats giving rain predominantly to the west coast. These complex weather patterns cause large-scale climate-induced coastal sedimentation during monsoon cyclones (Sangode et al. 2007). The large volumes of water flushing rivers during the monsoon purge and dilute anthropogenic pollution affecting the composition of sediment in the deltas of rivers that run through industrial areas (Alagarsamy and Zhang, 2010).
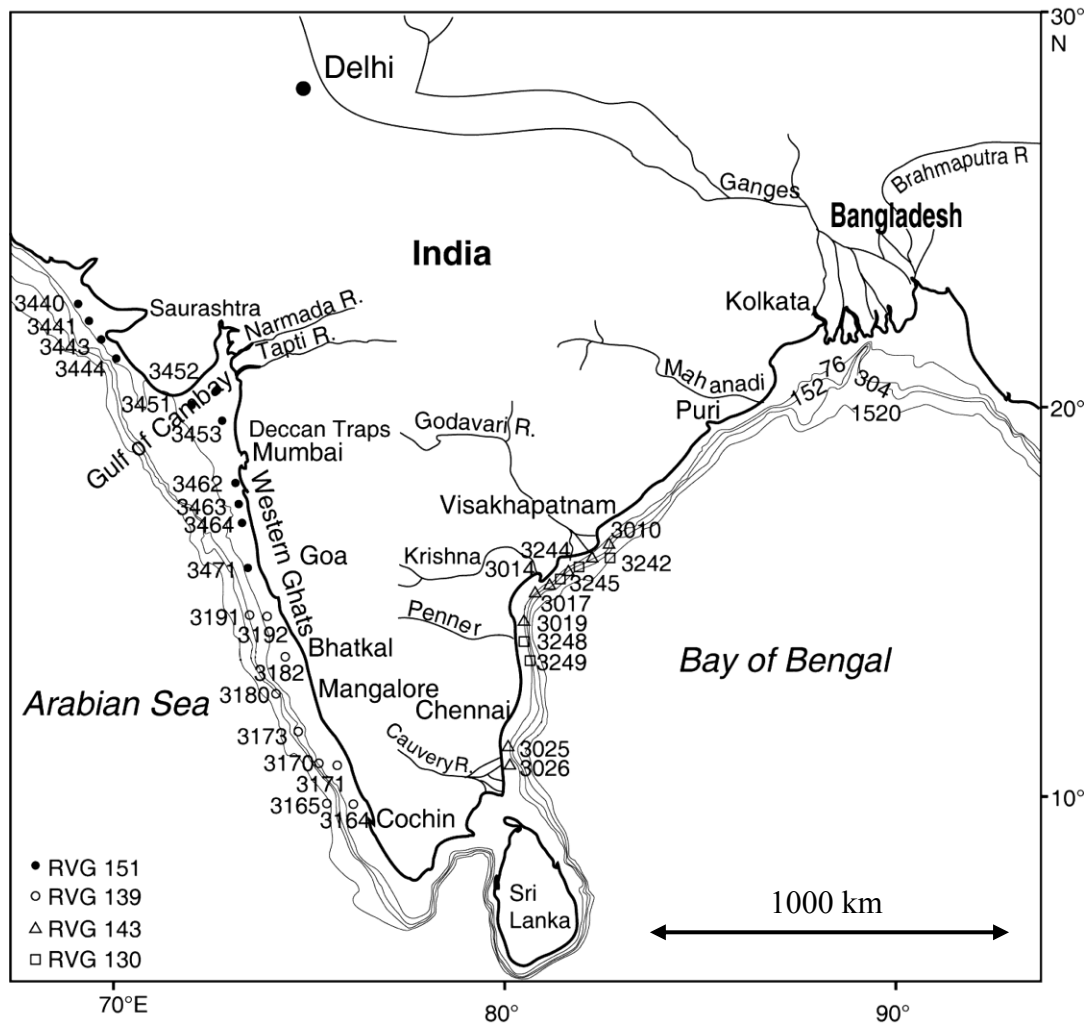

Fig. 1. Location of the principal rivers in the Indian peninsular and principal* sediment sampling stations on the Indian east and west coast during cruises RVG 130, 139, 143 and 151, see text, (some site labels omitted for clarity).

2.2 Coastal-geological setting

Source bedrock and their specific weathering mechanisms control the distinct geochemical compositions of Indian coastal sediments (Alagarsamy and Zhang, 2005). The outer limit of the eastern continental shelf lies at *c*. 200 m depth (Fig. 1) covered by calcareous relict sediment whilst the inner shelf and continental slope are covered by clastic sediments (Rao, 1985). Away from river mouths the shelves are covered by fine-grained terrigenous sediment. Sedimentation rates vary around the continental shelf, decreasing southwards along the WC. Deorukhakar (2003) observes 14 mm/yr in the Mumbai basin. Clay accumulation rate for the Gulf of Cambay are between 1.8 mm/yr and 19 mm/yr decreasing southwards from the confluence of the Tapti and Narbarda rivers (Borole 1988) to 0.01–2.6 mm/yr further southwest (Pandarinath et al. 2004), consistent with sediment dispersal being regulated by monsoon dominated littoral currents. Low clay accumulation rates (1.8–2.5 mm/yr) on the outer shelf suggest that transport of suspended matter across the shelf is low (Borole 1988). Very low sedimentation rates of 0.72 and 0.56 mm/yr at water depths of 35 and 45 m respectively have been determined by Manjunatha (1992) in the shelf region off Mangalore. The shelves formed at the mouths of northern east coast (EC) rivers receive a large part of their sediment from the Ganges, Brahmaputra and Mahanadi. Coastal sediments of the central EC region derive from the Godavari and Krishna. All these rivers form fertile deltas, which in turn, are heavily populated. These rivers have reduced the salinity of surface waters along the shore and, over time, their sediment load has resulted in shallow seas. Sediment input and annual discharge in the south is less from smaller rivers such as the Pennar and Cauvery (Rao, 1985). The Mahanadi, Godavari and Cauvery river systems discharge basaltic deposits into the EC Bay of Bengal due to the prevalence of Deccan Basalt within their catchments (Sangode et al. 2007). Sediments from rivers originating in the western part of India are derived from black "cotton soils" which cover the western Deccan Traps. In their lower reaches these rivers drain through Precambrian formations containing kaolinite rich soils. Black cotton soils are of secondary significance in the shelf sediments derived from the Godavari and Krishna rivers (Rao, 1991). The Indus is the largest source of sediment in the western Arabian Sea, extending outward from the coast to a distance of *c*. 1000–1500 km (Rao and Rao, 1995) to the north west of the current study area. The Indus predominantly drains the Precambrian metamorphic rocks of the Himalayas and to a lesser extent the semiarid and arid soils of West Pakistan and NW India (Krishnan, 1968). Deccan Trap basalts are the predominant rock types in the Saurashtra and drainage basins of the west coast (WC) Narmada and Tapti rivers. These rivers

discharge $\sim 60\times10^6$ tonnes of sediment annually through the Gulf of Cambay (Rao, 1975). The northern Western Ghats are composed of basalts between Mumbai and Goa, and further south, between Goa and Cochin, of Precambrian granites, gneisses, schists and charnockites (Krishnan, 1968).

Alagarsamy and Zhang (2005, 2010) have studied the occurrence of trace metals (e.g. Na, Mg, Al, K, Ca, Ti, Cr, Mn, Fe, Co, Ni, Cu, Ga, Ba, Pb) in suspension and sediment in the river mouths of major Indian rivers (e.g. Brahmaputra, Ganges, Narmada, Tapti, Krishna and Cauvery). They find that the average particulate trace metal concentration ($\sim 300 - 1000$ mg g^{-1}) to be higher than the global average ($\sim 170 - 350$ mg g^{-1}). Regional and watershed differences in segregation factors are observed, reflecting variable weathering rates due to differing mineralogy, preferential removal of alkaline and alkaline–earth metals relative to oxide-forming elements (e.g. Fe and Al), and a regional climatic shift from northern temperate to southern sub-tropical conditions. A study by Alagarsamy (2006) of the variation in anthropogenic input of trace metals (Fe, Mn, Co, Cu, Zn and Pb) into the industrialised lower Mondovi River and estuary shows that the seasonal influence (pre, during and post monsoon) upon metal concentration in the continental shelf is relatively small. Additional geographical, geological and climatic details of the Indian sub-continent may be found in Alagarsamy (2009).

3 Materials and methods

3.1 Sampling and analysis

Surface sediments from the east and west coasts of India were collected over a period of 14 months both before and after monsoon seasons along western and eastern portions of the Indian continental shelf during four cruises (130, 139, 143 and 151) of the R.V. Gaveshani (Table S1 in supporting information). The four digit station numbers in Table 1 (and Table S1), prefixed in the text and figures by S, are cross referenced in Fig. 1. Chronologically, sampling was undertaken along (i) EC in early January, post-Monsoon cruise 130, N to S, S3010 – S3026, (ii) WC late May / early June, pre-Monsoon, cruise 139, S to N, S3164 – S3192, (iii) EC early November, post-Monsoon, cruise 143, N to S, S3242 – S3249, (iv) WC March, pre-Monsoon, cruise 151, N to S, S3440 – S3471. Sediment samples were collected from the uppermost layer of the continental shelf at depths of between 30 and 700 metres using a deep-sea Van Veen Grab / Snapper. This sampled the surface layer to between 100 and 200 mm over an area of c. 1.2 m^2. Given the 0.56 to 19 mm/yr range of average sedimentation rates (Manjunatha 1992, Borole

1988, Deorukhakar 2003) this sample thickness represents the net sediment deposition at any given site of between two to ten years or so, which is longer than the experimental campaign period. As noted above, Alagarsamy (2006) found seasonal differences in anthropogenic trace metals in coastal sediments to be small. Thus the extended period of the sampling campaign is not expected to unduly bias the data set. Samples were bagged and frozen after collection to avoid cross contamination. After thawing and oven drying in the laboratory at $50 - 60^{\circ}C$ samples were disaggregated using an agate mortar. Bulk sediment samples were homogenised before subsampling for analysis. Nondestructive environmental magnetism measurements (using c. 15g) and EPR spectral measurements (using c. 0.01g) were undertaken prior to metals analysis by acid digestion (as detailed in supporting information). Environmental magnetism measurements were made on a subset of EC and WC samples. EPR spectra were subsequently modelled to elucidate the key magnetic components.

3.2 EPR spectral analysis

EPR spectra were obtained at room temperature in magnetic fields of 250±250 mT using a JEOL JES-TE100 spectrometer operating at a nominal frequency of 9.7 GHz with 100 kHz RF cavity modulation and digitised for analysis. Microwave power and modulation amplitude were adjusted to avoid saturation. Cavity modulation enables phase sensitive detection. This enhances the signal to noise ratio and results in spectra being detected as the differential of the absorption spectrum. Thus, symmetric Lorentzian or Gaussian resonances are displayed as anti-symmetric spectra with positive and negative peaks, their spectral g values determined from the baseline crossover field. The mean microwave frequency after cavity tuning was similar for all samples (9.355Ghz ±0.056%) resulting in base-line crossover for DPPH (g = 2.0036, S = ½) at 0.333T. DPPH was used as the standard for g-factor calculations. EPR spectra can be determined for a few milligrams or less of sample bestowing high sensitivity upon the technique. Spectra were normalised to experimental conditions (gain, microwave power and sample weight) permitting quantitative and qualitative comparison. Variations in the EPR differential signal intensity calculated by multiplying the linewidth, determined as the distance between the principle absorption maximum and minimum fields, dH_{pp}, by the peak to peak (PtP) signal amplitude, are often used as a proxy proportional to variations in relative concentration. This proxy has been compared to the total area of EPR absorption spectra, likewise proportional to the paramagnetic content of samples (see results and discussion). The total area of the EPR spectrum is a measure

of the para and ferri magnetic content of the samples contributed by magnetic particles and impurities. The intensity of six-line hyperfine Mn^{2+} EPR spectra was determined using the strongest low field resonance line (at ~ 325 mT) to minimise the effects of superposition from other spectral components around g ~ 2.00. When present in dilute samples, the Mn^{2+} hyperfine spectrum can be used as a secondary field calibration between spectra.

3.3 EPR applied to environmental sediments

   EPR is sensitive to paramagnetic ions with odd numbers of unpaired electrons. Zero field splitting appears in complexes which have more than one unpaired electron. Complexes with an odd number of electrons always give rise to an EPR spectrum (Abragam and Bleaney, 1970). Conversely, diamagnetic ions with even number of unpaired electrons do not exhibit EPR spectra. Classically, electron spins precess in a magnetic field at the Larmor frequency determined by the their spin and the field's magnitude. Resonance occurs when the simultaneous application of microwave photons of frequency, f, provides sufficient energy, E, to enable spin transitions between the Zeeman energy states. That is when the microwave and Larmor frequencies are equal such that $E = hf = g\mu_B\mu_0H$ where μ_B and g are the electronic Bohr magneton and g-value respectively. For dilute spin ½ ions a single resonance is observed with a g-value close to that of a free electron ($g_e = 2.0023$). Resonance can then be characterised by an effective g-value and its variation from that of a free electron by the shift in g, $\delta_g = g_{observed} - g_e$. g-shift is also a measure of the variation in the local field experienced by and perturbing the magnetic spin centres i.e. their magnetic and chemical environment. In strongly para- or ferri- magnetic sediments g-values can shift significantly above 2.00 as the sample magnetisation enhances the local field. The local field, however, only has limited capacity to move the resonance position of an EPR active species. Thus, resonances remote from g ~ 2 are more likely to be due to non s = ½ species. At constant (microwave) frequency the apparent g-value for dilute samples is inversely proportional to the resonance field, i.e. the EPR differential spectrum cross-over field. However, in more concentrated and multi-component samples the cross-over field approach to sediment impurity classification is naive as it cannot account for an admixture of several EPR active components or samples may be insufficiently dilute for the pure elemental g-value to be observed. Thus, spectral cross-over g-values may not be characteristic of all metals within a sediment and modelling of spectra is necessary if quantitative measurements are to be made. Further, for ferro- ferri- and anti- ferromagnetic particulate materials in sediments, the linewidth, and hence signal intensity, is dependent on particle size, shape and concentration. When even low concentrations of single,

pseudo single domain or polydomain ferri or ferromagnetic minerals are present, dipolar magnetostatic fields can cause line broadening of several hundreds of mT and consequently very broad and displaced EPR spectra (e.g. Crook et al. 2002). This is because intra- and inter-particle demagnetising and dipole-dipole fields perturb the high homogeneity EPR spectrometer field. Hence, in strongly magnetic environmental samples a linear relationship between magnetic susceptibility and EPR intensity cannot be assumed.

The microwave EPR magnetic susceptibility, DC, low (0.465kHz) and high (4.65kHz) RF magnetic susceptibilities measured using environmental magnetism methods (see sec.3.5 later) are all related by the sample's magnetic susceptibility tensor. Thus, taken together, these measurements have the potential to yield a characteristic 'fingerprint' of environmental sediments and contribute to source apportionment in sediment un-mixing models.

3.4 EPR modelling

Sediment EPR spectra have been modelled from first principles using a graphical user interface package developed at MMU, see supporting information for more detailed information. This enables the relative contribution from constituent components to be fitted and determined generating an EPR 'fingerprint'. This approach is more subtle and distinctive than using bulk environmental magnetism parameters alone. EPR spectrometer settings and sediment parameters comprise optimisable input (and consequently 'fingerprint') model parameters. Parameters include, for example, magnetic susceptibility and volume fraction, g-values and spin-lattice relaxation time, τ_1, of the para- and ferri-magnetic components. Hyperfine splitting and line broadening due to magnetostatic interactions, can be modelled using a number, n, of field-displaced resonances and optimising τ_1 such that the linewidths overlap. The model outputs the computed field dependent EPR absorption curve along with each resolvable magnetic component, determined on the basis of materially relevant sample characteristics. A model spectrum and its constituent components is shown in Fig. 2.
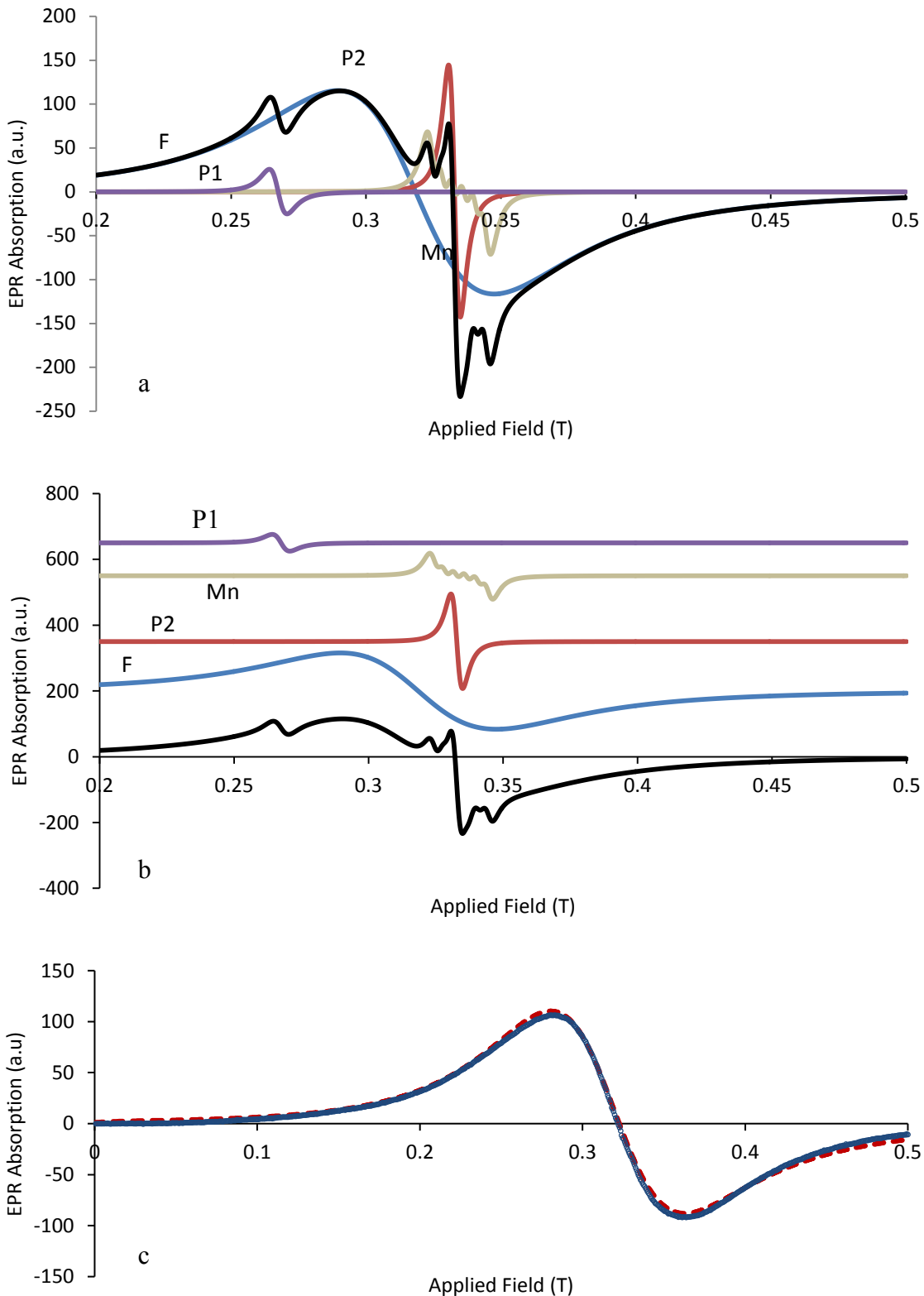
Fig. 2: a) An indicative composite model spectrum showing a broadline width particulate ferrimagnetic (magnetite) component (F), a six fold hyperfine paramagnetic (Mn^{2+}) and two paramagnetic components (P1, P2) of differing g- values, susceptibilities and volume fractions a) overlain spectrum, b) EPR spectrum components displaced for clarity, c) Experimental (solid line) and model fit (dashed line) for station R7-S3453 in the Gulf of Cambay.

3.5 Environmental magnetic methods

Only a summary of the environmental magnetic measurements and properties of these sediments sufficient to support the context and discussion of this EPR study is given here. For a detailed environmental magnetics study see Alagarsamy (2009), Alagarsamy and Zhang, (2010). Sample sizes for environmental magnetism measurements tend to be of the order of several grams or tens of grams rather than a few milligrams as for EPR. In environmental magnetism, determination of the so called Low Frequency (LF) 0.465kHz and High Frequency (HF) 4.65kHz RF susceptibilities and their difference ratio, χ_{fd} (%), are used as a measure of the presence of superparamagnetic mineral grains. High LF and HF susceptibility, suggests the presence of significant ferri- or para- magnetic content. Paramagnetic Fe^{3+} and Mn^{2+} ions, which result in high environmental magnetism susceptibility are expected to show strong EPR spectra. Increased LF and HF susceptibility is associated with discharge from the Krishna and Visakhapatnam delta. Alagarsamy (2009) observed that magnetic susceptibility had a more significant coefficient of determination (R^2 = 0.91–0.98) with the concentration of transition metals Fe, Cr, Cu and Ni in EC sediments which also have higher concentration of ferrimagnetic minerals. EC samples showed higher values of χ_{fd}(%) consistent with the presence of finer ferrimagnetic grains and enrichment of ferrimagnetic minerals also resulting in higher values of Isothermal Remanent Magnetisation (IRM), Saturation IRM (SIRM) and magnetic susceptibility suggesting the presence of higher ferrimagnetic minerals possibly derived from the weathering of Deccan Basalts (Alagarsamy 2009). EC samples also show greater correlation between and the magnetic susceptibility parameters (χ, χ_{ARM}, $IRM_{20\ mT}$ and SIRM) and Fe, Cr, Cu and Ni concentration (Alagarsamy, 2009).

4 Results and discussion

4.1 Metal concentrations

A detailed study of the geochemical distribution of the major and minor trace elements in these sediments (as listed in Sec.2.2) may be found in Alagarsamy and Zhang (2010). Here we report the IAS data of the paramagnetic elements relevant to EPR (i.e. Fe, Cu, Cr and Ni) in order to place the EPR spectra and environmental magnetic measurements in context. Of these four paramagnetic impurities Fe dominates the sediments at concentrations between 1 and 10 wt%, followed by Cu (4–140 ppm), Cr (1–130 ppm) and Ni (0.3–80 ppm), Fig. 3, Table S2. Fig. 3

displays the coastal metal concentrations geographically at survey stations along the continental shelf. Correlation between Cr, Ni, Cu and Fe are visually striking and statistically highly significant (Pearson correlation coefficients between 0.776 and 0.936, Fig. S1) consistent with entrainment of Cr, Ni, Cu with Fe in all sediments. Enhanced metal concentrations indicative of anthropogenic pollution (e.g. Cr, Ni) are observed in both western and eastern deltaic and coastal regions of the major river systems draining from the major basaltic rich catchments, Fig. 3. The broken horizontal lines in Fig. 3 correspond to the threshold concentration ranges for 'low' / 'medium' biological effects for Ni (20.9 / 51.6 ppm), Cu (34 / 270 ppm) and Cr (81 / 370 ppm) as defined by Long et al. (1995). Whether using the 'low' or 'medium' threshold concentration levels for Ni as a proxy for biologically significant levels of anthropogenic pollution, it is seen from Fig. 3 that the most biologically polluted sediment systems lie on the WC between the Saurashtra and northern Mid-Western Ghats and on the EC from the Penner to the Krishna and Visakhapatnam. Distal from these large river catchments (i.e. from the Western Ghats, through Mangalore, to Cochin and to the eastern Cauvery catchment) the sediments are generally far less impacted with Ni levels below the 'low' biological impact threshold. In the region of the Visakhapatnam Deltaic the high trace metal concentrations are almost identical for shallow (76 m and 152 m) and deep (1520 m) stations implying extensive sediment dispersal down the steep continental shelf. That is, bio-toxic concentrations of metals of anthropogenic origin impact well beyond the shallow coastal margin. In contrast, neither shallow nor deep station sites in the non-deltaic Cochin region on the SW coast, are significantly impacted, exhibiting only very low levels of Ni (0.32ppm).
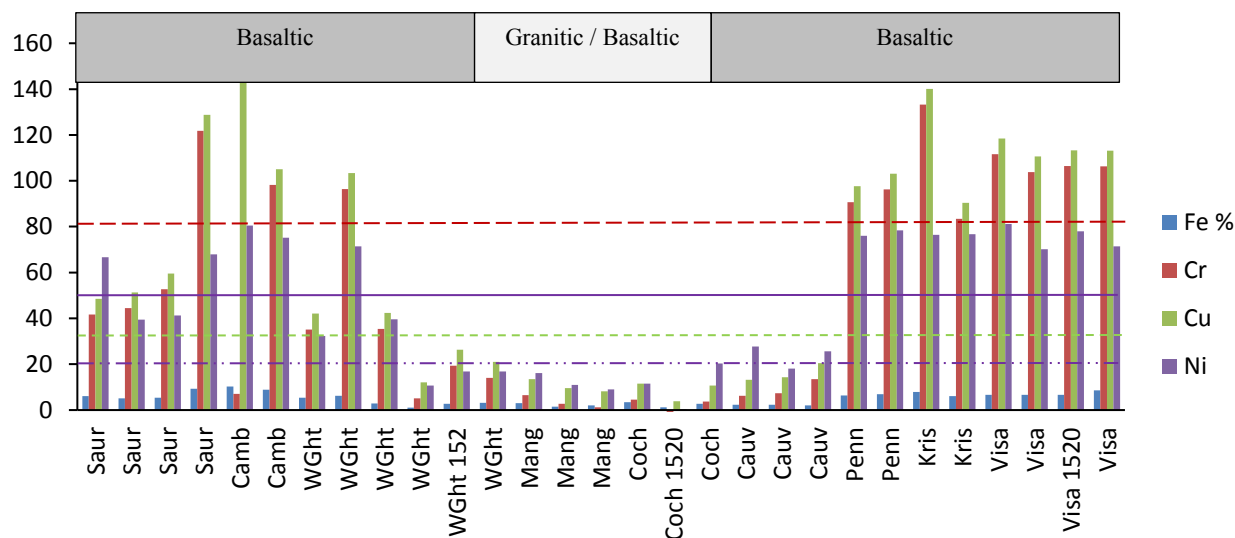
Fig. 3: Coastal sediment distribution of Fe (wt%), and Cr, Cu and Ni (ppm). Horizontal lines, in ascending order, correspond to i) low biological effect for Ni(- - 20.9ppm), Cu(− − 34ppm) and Cr(− ·· − 81ppm), and ii) the medium effect range (solid line) for Ni (51.6ppm).

4.2 EPR spectral characteristics and parameters

Differences in EPR spectra can be associated with the presence, oxidation state and concentration of para- and ferri- magnetic impurities. The impurities observed in the EPR spectra are mainly paramagnetic Mn^{2+} and Fe^{3+}, (Fig. 4). Fig. 4a shows the distinctive Mn^{2+} six line hyperfine resonance spectrum taken from an expanded central section of the EPR trace for SW Ghats station R12-S3191. Compared to pure Mn^{2+} the spectrum is displaced vertically and horizontally by other (e.g. Fe) components in the sample. As the spectra have been normalised, then for paramagnetic ions of similar linewidths, peak intensity roughly corresponds to the relative concentration of the impurity. The paramagnetic components centered at g ~ 2.00 are primarily indicative of Mn^{2+} although spectral contributions from any Fe^{3+}, free radicals in organic carbon or free electron centres in carbonates also occur at g ~ 2.00. The difference between Mn^{2+} and Fe^{3+} is that the latter has a broad resonance peak without any hyperfine resonances. This general information, enables the classification of the magnetically active transition metal centres as indicated in Table 1. Of the metal ions present in these samples only [55]Mn and [63,65]Cu have non-zero nuclear spins (5/2 and 3/2 respectively) and sufficient magnitude to provide hyperfine coupling splitting of the EPR spectrum resulting in 6 and 4 hyperfine resonance lines respectively. Due, however, to dipole-dipole interactions from Fe, hyperfine

resonance structure tend to occur as broad resonance lines. Similarly we do not expect to detect weak E_1' centres above the general broadline background in these light exposed samples measured at room temperature. Table 1a shows the relatively small variation in spectral g-values ($\delta g < 0.294$) determined from the cross-over field as well as the concentration of metal ions present in the sediments. No simple correlation is observed in these complex sediments between the concentration of elemental iron, for example, and the corresponding magnitude of distinctive Fe^{3+} absorption lines, nor between g-value (shift) and elemental concentration.

Table 1: EPR model parameter values for reported spectra. a) K is the principal uniaxial anisotropy constant (kJm^{-3}), α the ferrimagnetic damping constant, τ_{1n} (n 1 to 3) are paramagnetic spin-lattice damping times, EPR g-factors g_n, b) ferri- and para- magnetic volume / susceptibility products $V_f.\chi_f$ and $V_{pn}.\chi_{pn}$, respectively, (n = 1 to 3) are the number and splitting, μ_0H_{fn} (mT) of the hyperfine fields. Not detected (n.d.).

a)

S-E Rank index R	Station ID S	Coastal Region	Dominant Spectral Shape & Strength	spectral g-value	Ion	K (kJ/m³)	α	$\tau_{1.1}$ (mS)	$\tau_{1.2}$ (mS)	$\tau_{1.3}$ (mS)	g_1	g_2	g_3
1	3440	Saur.	Single, broad, weak	2.119	Fe^{3+}	1.00	0.23	0.100	4.000	0.200	5.500	1.980	4.000
2	3441	Saur.	Single, broad, weak	2.067	Fe^{3+}	1.00	0.23						
3	3443	Saur.	Single, broad, medium	2.128	Fe^{3+}	2.50	0.23	0.100			2.500		
4	3444	Saur.	Single, broad, strong	2.100	Fe^{3+}	2.00	0.20						
6	3452	Camb.	Single, broad, strong	2.097	Fe^{3+}	1.00	0.20	0.100			2.150		
7	3453	Camb.	Single, broad, strong	2.074	Fe^{3+}	1.30	0.19	0.100			2.000		
8	3462	Mumb.	Single, broad, strong	2.086	Fe^{3+}	1.90	0.19						
9	3463	Mumb.	Single, broad, medium	2.127	$Mn^{2+} Fe^{3+}$	2.00	0.23	0.100			2.500		
10	3464	WGha.	Single, broad, medium	2.059	Fe^{3+}	0.60	0.23	0.100	0.200		2.000	4.050	
12	3191	WGha.	V Weak, Weakly resolved	2.271	Mn^{2+}	0.02	0.10	0.080	8.000	0.060	2.350	2.005	2.000
13	3192	WGha.	Single, Weak	2.254	$Mn^{2+} Fe^{3+}$	7.00	0.14	0.080	1.000		2.350	2.900	
14	3182	Bhatkal	Weak, Weakly resolved	2.135	low Fe^{3+}	8.00	0.23	0.100	0.400		2.000	2.600	

15	3180	Mang.	multi, broad	2.025	low Fe^{3+}	0.10	0.23	0.100	4.000	0.200	2.200	1.980	4.000
16	3173	Mang.	Weak, Weakly resolved	n.d.	n.d.	0.02	0.19	0.075	0.175		2.600	2.800	
17	3170	Cochin	Multi, weak	2.251	Mn^{2+}	0.02	0.19	0.075	0.175		2.600	2.800	
19	3165	Cochin	Multi, v. weak	2.050	low Mn^{2+} Fe^{3+}	0.02	0.22	1.000	0.300	0.180	2.230	2.200	2.250
20	3164	Cochin	Weak, Weakly resolved	n.d.	n.d.	1.00	0.25	0.100	8.000	0.475	2.300	2.005	3.700
21	3026	Cauv.	Multi, weak	2.115	$Mn^{2+}Fe^{3+}$	0.80	0.23	0.100	0.060		3.100	4.800	
22	3025	Cauv.	Multi, weak	2.195	low Fe^{3+}			0.170			4.600		
23	3024	Cauv.	Multi, v. weak	n.d.	n.d.	10.00	0.23	0.080	0.050	0.100	2.050	5.200	3.800
24	3249	Penner	Single, broad, weak	2.102	Fe^{3+}	1.00	0.23						
25	3248	Penner	Single, broad, medium	2.089	Fe^{3+}	1.00	0.21						
26	3019	Penner	Single, broad, medium	2.093	Fe^{3+}	0.02	0.18	0.080	0.060		2.200	2.600	
28	3014	Krishna	Single, broad, medium	2.296	Fe^{3+}	6.00	0.23	0.100			2.600		
29	3245	Visa.	Single, broad, medium	2.119	Fe^{3+}	2.00	0.23	0.100	8.000	0.475	2.300	2.005	3.700
30	3244	Visa.	Single, broad, medium	2.038	low Fe^{3+}	0.07	0.19	0.150			2.000		
32	3013	Visa.	Single, broad, medium	2.092	Fe^{3+}	0.02	0.20	0.080	0.060		2.200	2.600	
33	3012	Visa.	Single, broad, medium	2.119	Fe^{3+}	0.02	0.18	0.080	0.060		2.250	2.600	
34	3010	Visa.	Single, broad, medium	2.044	Fe^{3+}	0.02	0.19	0.150			2.000		

N-S-E Rank index R	Station ID S	Coastal Region	$V_f.\chi_f$	$V_{p1}.\chi_{p1}$	$V_{p2}.\chi_{p2}$	$V_{p3}.\chi_{p3}$	n_1	n_2	n_3	$\mu_0 H_{f1}$ (mT)	$\mu_0 H_{f2}$ (mT)	$\mu_0 H_{f3}$ (mT)
1	3440	Saur.	4.0E-04	4.8E-07	2.0E-09	1.5E-07	1	6*	1		10	
2	3441	Saur	3.7E-04									
3	3443	Saur.	3.6E-03	3.2E-05			25			9		
4	3444	Saur.	7.2E-03									
6	3452	Camb.	3.1E-02	3.2E-03			7			10		
7	3453	Camb.	8.4E-03	9.0E-05			1					
8	3462	Mumb.	6.0E-03									
9	3463	Mumb.	7.6E-04	3.2E-05			25			9		
10	3464	WGha.	1.1E-03	1.3E-05	1.5E-07		1	1				
12	3191	WGha.	1.0E-05	1.5E-05	1.0E-10	5.0E-06	5	6*	7	30	10	40
13	3192	WGha.	4.0E-05	2.5E-05	1.0E-08		5	1		30		
14	3182	Mang.	6.0E-05	9.6E-06	1.0E-07		7	1		10		
15	3180	Mang.	6.0E-05	9.6E-06	3.0E-09	1.0E-07	11	6*	1	15	10	
16	3173	Mang.	4.0E-05	4.0E-06	2.5E-07		1	1				
17	3170	Cochin	4.0E-05	4.0E-06	2.5E-07		1	1				
19	3165	Cochin	1.0E-04	5.0E-08	4.0E-07	5.0E-06	4	1	1	10		
20	3164	Cochin	3.0E-05	1.6E-06	1.0E-10	5.0E-08	7	6*	1	10	10	

| No	ID	Name	V1	V2	V3	V4	V5	V6	V7	V8	V9
21	3026	Cauv.	4.6E-04	3.2E-06	1.5E-05		1	1			
22	3025	Cauv.	0.0E+00	2.0E-06			1				
23	3024	Cauv.	1.0E-05	1.6E-05	1.0E-05	1.0E-06	1	15	1		10
24	3249	Penner	1.0E-03								
25	3248	Penner	5.0E-03								
26	3019	Penner	1.4E-03	1.3E-04	3.0E-05		1	1			
28	3014	Krishna	4.0E-03	1.6E-04			25			9	
29	3245	Visa.	7.0E-03	1.6E-06	1.0E-10	5.0E-08	7	6*	1	10	10
30	3244	Visa.	2.0E-03	4.5E-05			1				
32	3013	Visa.	2.7E-03	2.0E-04	1.0E-04		1	1			
33	3012	Visa.	1.6E-03	1.7E-04	5.0E-05		1	1			
34	3010	Visa.	8.0E-04	5.0E-06			1				
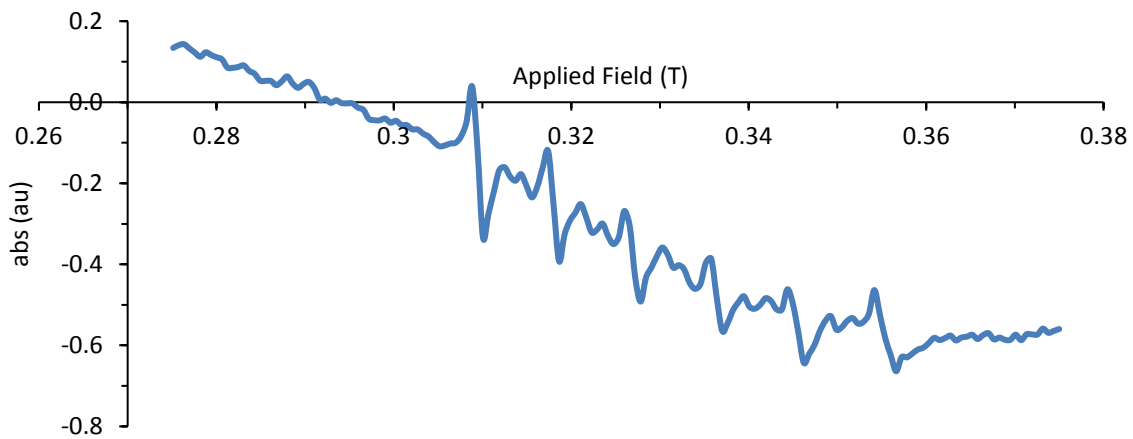
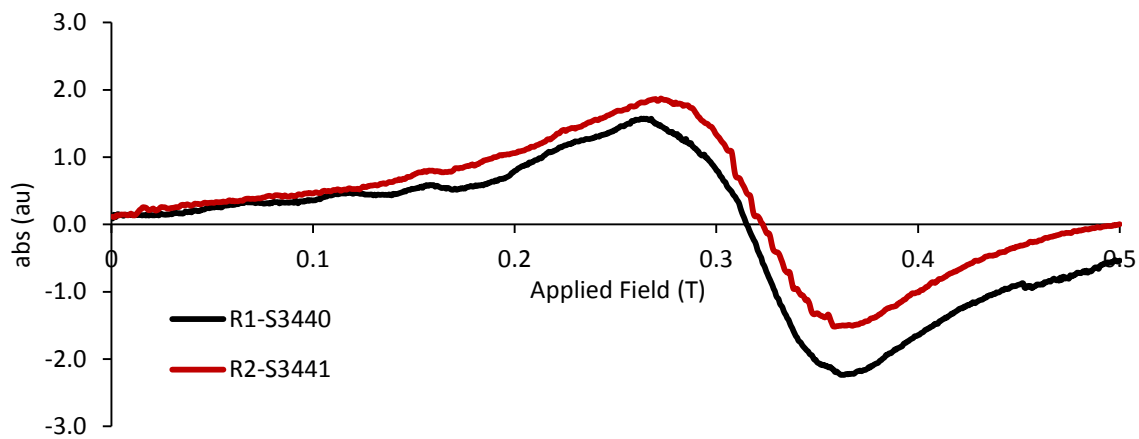Fig. 4a: Mn^{2+} hyperfine absorption component, an expanded central section of S 3191.

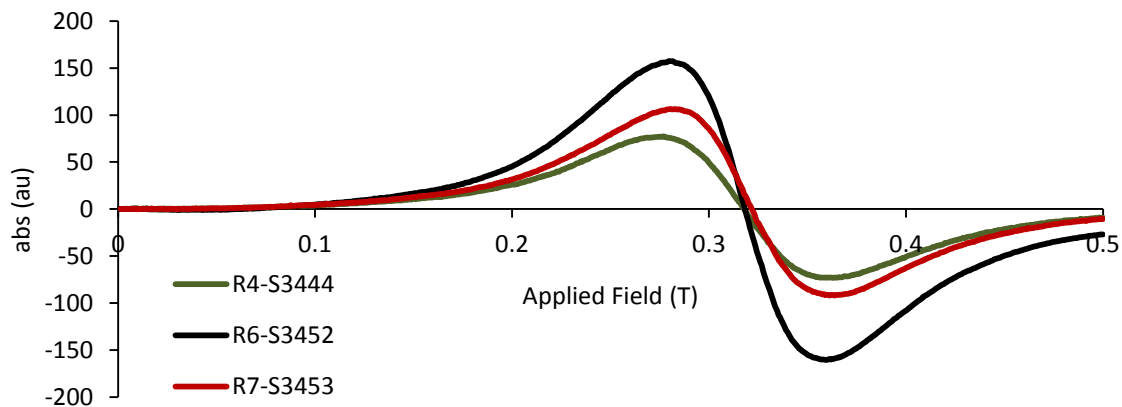Fig. 4b: Proximal R1-S3440 & R2-S3441, N Saurashtra Basin, with low PtP values ~3.5a.u.

Fig. 4c: R4-S3444: S Saurashtra Bay, and 400km distant R6-S3452, R7-S3453 N & S Gulf of Cambay, respectively. Strong PtP ~200a.u., broadline spectra, similar spectral g-values.
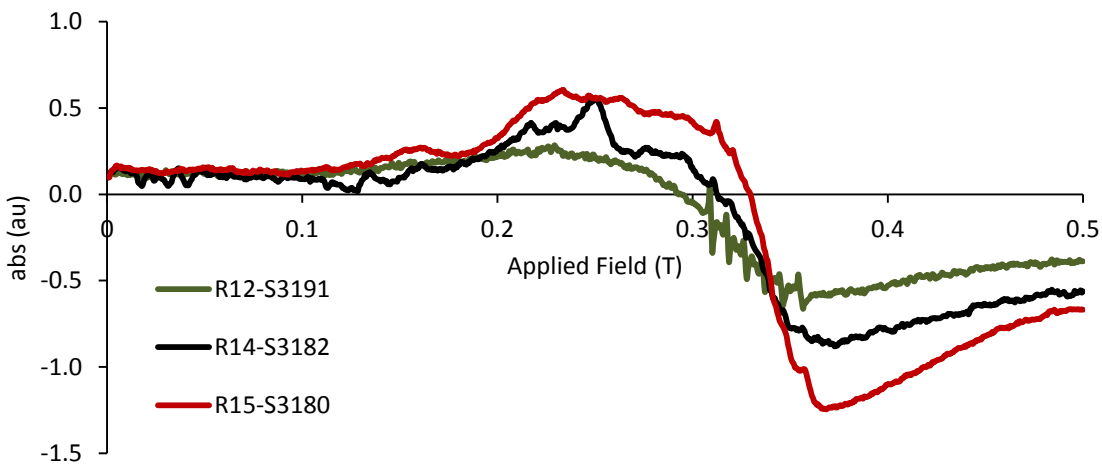
Fig. 4d: R12-S3191, SW Ghats, R14-S3182 Bhatkal & R15-S3180 Mangalore, low PtP values ~1.0a.u., unimpacted sites. Note Mn^{2+} hyperfine spectrum in R12-S3191.
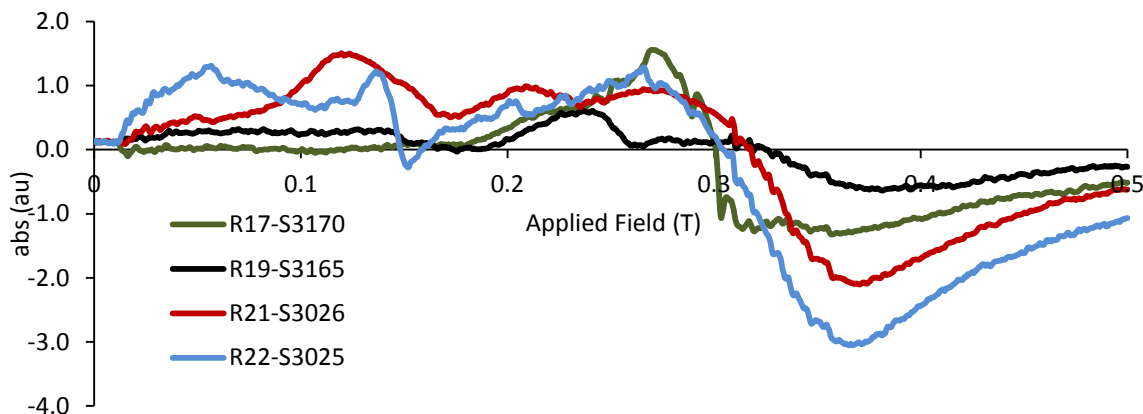

Fig. 4e: Multicomponent WC R17-S3170, R19-3165 N & Central Cochin resp., EC R21-S3025 & R22-S3026 N Cauvery delta spectra, low PtP, between 1 & 4a.u.
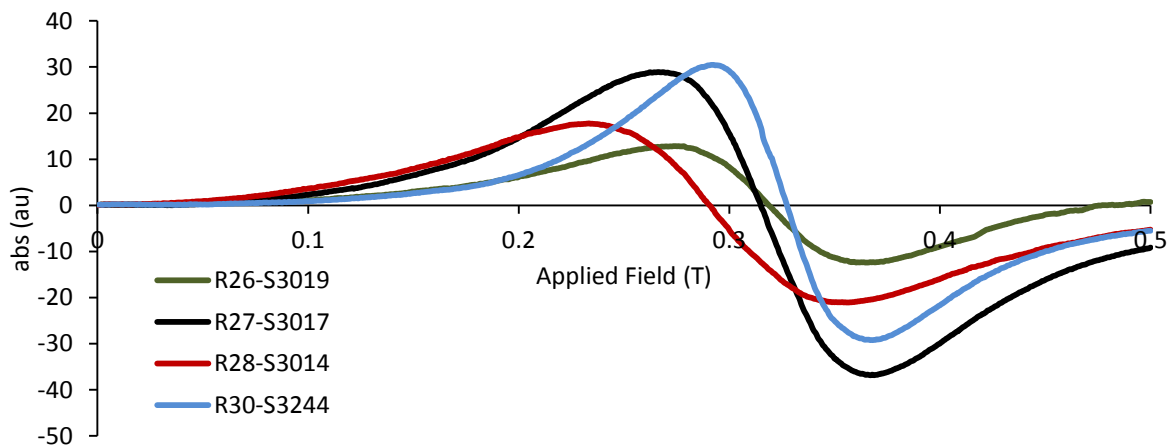

Fig. 4f: EC R26-S3019 N Penner, R28-S3014 & R27-3017 Krishna, R30-3244 S Visa delta, moderate strength broadline spectra (25 to 65a.u.) and significant spectral g-shifts.

In Fig. 4b-f indicative spectra have been grouped broadly by station coastal location. For visual clarity not all spectra are included. The spectra exhibit a variety of visual forms and amplitudes reflecting potential variation in the total concentration of para-, ferri- and canted antiferro- magnetic components. In some samples strong fairly uniform, weakly field dependent spectra are observed, e.g. Fig. 4e. Commonalities in the gross spectral characteristics, and thus by implication the sediment, are however evident as is now discussed.

Fig. 4b shows low PtP values of ~ 3.5a.u for R1-S3440 and R2-S3441 from the WC North Saurashtra Basin, stations well sheltered from the influence of the more southerly discharges from the Gulf of Cambay. A weak Mn^{2+} hyperfine signature is seen in R2-S3441.

Fig. 4c: shows, strong PtP ~ 200a.u., broadline peaks with similar g-values from R4-S3444 S Saurashtra Bay, and proximal (*c*. 400km) R6-S3452 and R7-S3453 from north and south of the Gulf of Cambay, respectively. These strong, large, broadline spectra are potentially influenced by discharges from the WC Gulf of Cambay. Similar EPR spectral characteristics are displayed for coastal stations down to the northern extremities of the Western Ghats. They exhibit strong EPR absorption consistent with ferrimagnetic minerals being present in moderate concentrations (i.e. here between 9 to 10 ppm, Fig. 1). All broadline spectra (e.g. WC Fig. 4c and EC Fig. 4f) are typical of sediments associated with high para or ferrimagnetic content, that is from river catchments or coastal locations proximal to highly populated regions generating anthropogenic pollutants.

In Fig. 4d and e no single EPR spectral component dominates enabling the weaker impurities to be clearly resolved and characteristic Mn^{2+} and broadline Fe^{3+} (ferric) components to be seen. Fig. 4d displays weaker multicomponent spectra, R12-S3191, from the SW Ghats and R14-S3182 and R15-S3180 from Bhatkal and Mangalore stations, representing a site separation range of *c*. 150 km. They have low PtP values (*c*. 1.0 a.u.), characteristic of unimpacted continental shelf sites consistent with lower total impurity content, (i.e. here low Fe concentrations of between 1 and 2.7 ppm). The lower overall level of iron rich material means that the weaker narrow line components are more clearly resolved and contribute to a larger percentage of the overall spectral absorption. The Mn^{2+} hyperfine signature is particularly clear in R12-S3191 more weakly in R13-S3192, consistent with lower levels of anthropogenic pollution and riverine sediments. Both the of the latter two stations are situated in the west coast SW Ghats region remote from the outfall of major rivers or deltas.

Fig. 4e displays weak multicomponent spectra from either side of the Southern Indian peninsular, i.e. west coast R17-S3170 and R19-3165 from the N and Central Cochin respectively,

and east coast R21-S3025 and R22-S3026 from the N Cauvery Delta. For R22-S3025 a clear Fe^{3+} peak is seen at g = 4.6, (see also Table 1) at ~ 0.15T, comparable to g = 4.7 Fe^{3+} peaks observed by Engin et al. (2006) in powdered fossil gastropod shell at room temperature. The spectra display a strong fairly uniform, weakly field dependent behaviour below g ~ 2. Similar behaviour is exhibited by the Cauvery Delta stations R23-S3024 and R24-S3025, Cochin R20-S3164 and R19–S3165, and Mangalore R16-S3173 (spectra not shown for visual clarity). These sediments all display low to medium PtP, between 1 & 4a.u., and characteristics similar in to those of Fig. 4f. The stations which are adjacent to the northern Cauvery delta are very low in para and ferrimagnetic components consistent with their low Fe concentrations of between 2.2 and 2.8 ppm.

Figs. 4f shows moderate strength spectra (amplitudes of 25 to 65 a.u.) from the east coast, R26-S3019 N Penner, R28-S3014 and R27-3017 Krishna estuary and R30-3244 from the S Visakhapatnam Delta region, representing a site range of *c*. 150 km. The spectra are visually similar to those of Fig. 4b but with strong g-shifts, δ_g, of ~ 0.6, for R33-S3012, R32-S3013, R28-S3014, (not all spectra displayed) and Table 1. Spectra from Krishna (R28-S3014) and the South Visakhapatnam delta / North Krishna (R30-S3244 and R29-S3245, spectrum not displayed) with δ_g ~ 1.7 are consistent with lower Fe^{3+} concentrations, here between 6 and 8 ppm.

4.3 EPR modelling parameters

Modelling EPR spectra enables the semi-qualitative classification of sediments discussed above to become quantitative. It also permits spatial association and variation to be studied in greater detail. Table 1 displays the principal modelling parameters that provide a good fit to the experimental spectra replicating peak positions with the overall area of fitted and experimental spectra differing by no more than a few percent (e.g. Fig. 2c, R7-S3453, Gulf of Cambay). It is seen from Table 1b that some spectra, such those of the Bhatkal/Mangalore stations (i.e. R14-S3182, R15-S3180, R16-S3173), require both a ferri- and at least one para- magnetic component, to accurately replicate the experimental spectra. In contrast, other stations, such as the two southern most EC Penner stations, (i.e. R26-S3019) can be modelled using a single ferrimagnetic component. The ferrimagnetic uniaxial anisotropy constant, *K* (kJm^{-3}), is typically found to be similar in magnitude to that of magnetite. The ferrimagnetic damping constant, α, increases for broader absorption lines. The paramagnetic spin-lattice relaxation times, τ_{1n} (n = 1 to 3), are longer for narrow intense lines consistent with a dilute or weaker magnetic environment, e.g. τ_{13}

= 4 mS for R1-S3440, R12-S3191, R20-S3164. The ferri- and para- magnetic volume and susceptibility products, $V_f.\chi_f$ and $V_{p1}.\chi_{p1}$ respectively of Table 1b, are proportional to the contribution that a component makes to the total EPR absorption. It is clear from Fig. 5a that the largest ferrimagnetic concentrations and susceptibilities are associated with the most intense EPR spectra corresponding to stations in the west coast NW Gulf of Cambay and east coast Visakhapatnum delta. This is consistent with the high values of Fe, determined by ICP. The g-factors, varying here from 2 to 5.5, are determined both by the paramagnetic impurity and its local environment, shifting to low fields (higher g) as the mean field from other magnetic components increases. Parameters n and H_f are the number and hyperfine splitting field (in mT), respectively, necessary to either reproduce a Mn^{2+} hyperfine absorption or simulate a broadened paramagnetic absorption component with shortened spin-lattice relaxation times. Examples of overlapping traces simulating a broad paramagnetic absorption are $n_1 = 5$, $n_3 = 7$, $H_f = 30$ mT and 40 mT for R12-S3191 and $n1 = 11$ $H_f = 15$ mT for R15-S3180. Here Mn hyperfine absorption (flagged in Table 1 by $n_2 = 6*$) has been modelled using $H_f = 10$ mT, e.g. R1-S3440, R12-S3191. A wide range of paramagnetic impurity g-values is observed. The largest, 5.5, occurring at the most northerly Saurashtra station, R1-S3440, is probably due to the presence of ferrimagnetic minerals. If both ferrimagnetic and paramagnetic minerals are present only when their EPR contribution is comparable or when the paramagnetic component is dominant, are paramagnetic species and likely to be readily resolvable.

Figs. 5b and 5c display the coastal geographical trends in principal paramagnetic components and the departure from g = 2 determined by EPR modelling. The largest paramagnetic components (Fig. 5b) are associated primarily with the larger WC rivers and EC deltaic margins. The principal ferri- and para- magnetic components are displayed in in these two figures as the products of the component's susceptibility and volume fraction, $V_f.\chi_f$ and $V_{p2}.\chi_{p2}$, as it is this product which determines their contribution to the EPR spectrum. Fig. 5c displays up to three g-values per spectrum. Consistent with the discussion above, no simple correlation between g-values and total EPR absorption is observed due to spectral g-values being dependent upon both the specific sediment composition and concentration.
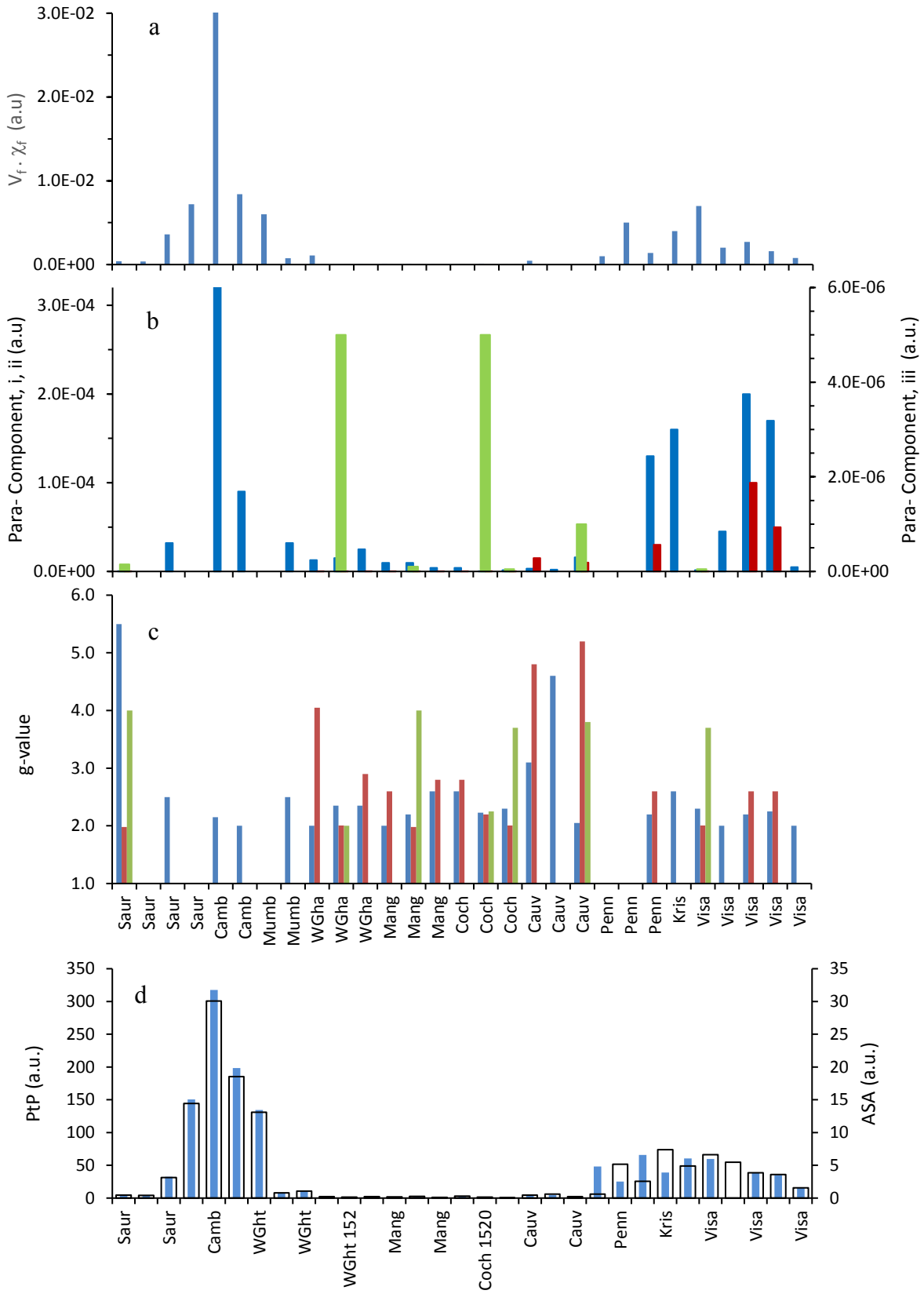
Fig. 5: Geographical variation in a) ferrimagn. $V_f \cdot \chi_f$, b) dominant paramagn. $V_p \cdot \chi_p$: i ■, ii ■, iii ■. c) paramagn. g-values g_i ■, g_{ii} ■, g_{iii} ■, d) PtP (solid) and ASA (open) bars.

The geographical correspondence by station location of EPR absorption spectral area (ASA) and PtP (Fig. 5d) is similar, but not identical to, those of the impurity concentrations (Fig. 3). The correlation coefficients between ASA and PtP with total impurity concentration over all samples is similar, 0.707 and 0.673 respectively, thus some difference in the form of the geographical distribution of these parameters is to be expected. We find ASA and PtP to be highly correlated with $r^2 = 0.980$ (Fig. S2). Below 100 ppm a weaker correlation is observed between PtP, ASA and impurities. ASA vs its proxy, $tP \times dH_{pp}$, also has a very high correlation coefficient of 0.97. For pure single component materials dH_{pp} is expected to be negatively correlated with concentration due to strengthening of magnetostatic dipole-dipole interaction fields. Negative weak correlation between dH_{pp} and impurity concentrations (i.e. Fe -0.577, Cu -0.492, Cr -0.528, Ni -0.546) are observed for these multi-component sediment samples. We find weaker (negative) correlation is shown between dH_{pp} and both EPR area (-0.324) and PtP height (-0.315). Also, the correlation between ASA and total metal content is weak (r = 0.109) at low impurity levels (< 4.5 wt%), but greater (r = 0.67) above 4 wt% (Fig. S3). The Pearson correlation coefficients between ASA and impurity concentration over all stations are ASA-Fe = 0.707, ASA-Cu = 0.652, ASA-Ni = 0.506 and ASA-Cr = 0.472. The low total metal content / low ASA stations all lie between the Southern Western Ghats through Cochin, around the southern Indian peninsular and northwards as far as the Penner River. That is, away from the Gulf of Cambay and the Eastern Krishna and Visakhapatnum. These low total metal concentration stations also display characteristically weaker multicomponent EPR spectral signatures. Slightly over half of these stations (R12-S3191 to R20-S3164) have sediment input associated with granites and gneiss, the remainder (R21-S3026 to R25-S328) with basaltic sediments (Table S1). This geological difference does not, however, appear to determine the EPR absorption (or the magnetic susceptibility, see section 4.4 below).

For lower impurity concentrations the peak width, $\mu_0 dH_{pp}$ (T), clusters around two principal values when samples are classified by total impurity concentration (Fig. S4). This may suggest that a single species is predominantly responsible for these linewidths. This behaviour is consistent with the complementary case for four outlying points ($\mu_0 dH_{pp} > 0.24$ T) for low total impurity multicomponent concentrations (<50 μg/g). Low concentrations of impurities with differing g-values can result in spreading of the partially resolved weak spectral components over a relatively wide field range effectively broadening the composite spectrum of the sample. The values of δ_g determined by the difference between the spectral cross-over field and g = 2 possess

no simple geographical dependence, being largely determined by the dominant components found at any given station (Fig. 6a). The maximum and mean shifts observed, 0.294 and 0.125, respectively, are much smaller than those determined from modelling the g-values of individual components. That is, in these multicomponent environmental sediments the g-value determined from spectra cross-over is not primarily dependent upon one dominant impurity as the contribution of several broadline components may determine the composite sediment spectrum. This is consistent with no significant or analytically consistent correlation being observed between δ_g and composition. Thus, overall we do not consider δ_g to be a robust proxy parameter for impurity level due to superposition of multiple components within the spectra in complex environmental sediments.

4.4 Comparative environmental magnetism measurements

Fig. 6b demonstrates that between the Western Ghats and Visakhapatnum, the environmental magnetism LF and LF magnetic susceptibilities (Table S3) are greatest in the regions associated with the Krishna and Visakhapatnum, sources of anthropogenic pollution and watersheds in which Deccan Basalt occur such as those above the tributaries of the Godavari. We find very strong correlation coefficients between LF and HF susceptibilities and primary EPR spectral parameters (ASA in particular) and metal impurities, (Table 2). HF and LF are themselves highly correlated (0.999) by the function HF = 0.97LF, (see also Alagarsamy 2009). The small difference between LF and HF indicates that there are relatively few fine grained superparamagnetic particles in these coastal marine sediments. This is not perhaps surprising as such particles are more susceptible to bio-chemical uptake, oceanic dispersal and oxidation and so likely to have shorter chemically unaltered residence times either on the continental shelf or in the river catchment. Further, Fe, Cr, Cu and Ni are strongly correlated, (Table 2, Fig. S1). A strong correlation between high magnetic susceptibility and heavy metal concentration is consistent with the fact that magnetic iron and manganese oxides are commonly found in close association with clay minerals which have a strong absorptive capacity for metals (Alagarsamy and Zhang, 2010, Kersten and Smedes, 2002). The geographical distribution of ASA and the high correlation factors exhibited between ASA, LF and HF, give confidence that the extra fingerprinting capability of EPR is consistent with more conventional environmental magnetism methodologies and chemical assay.
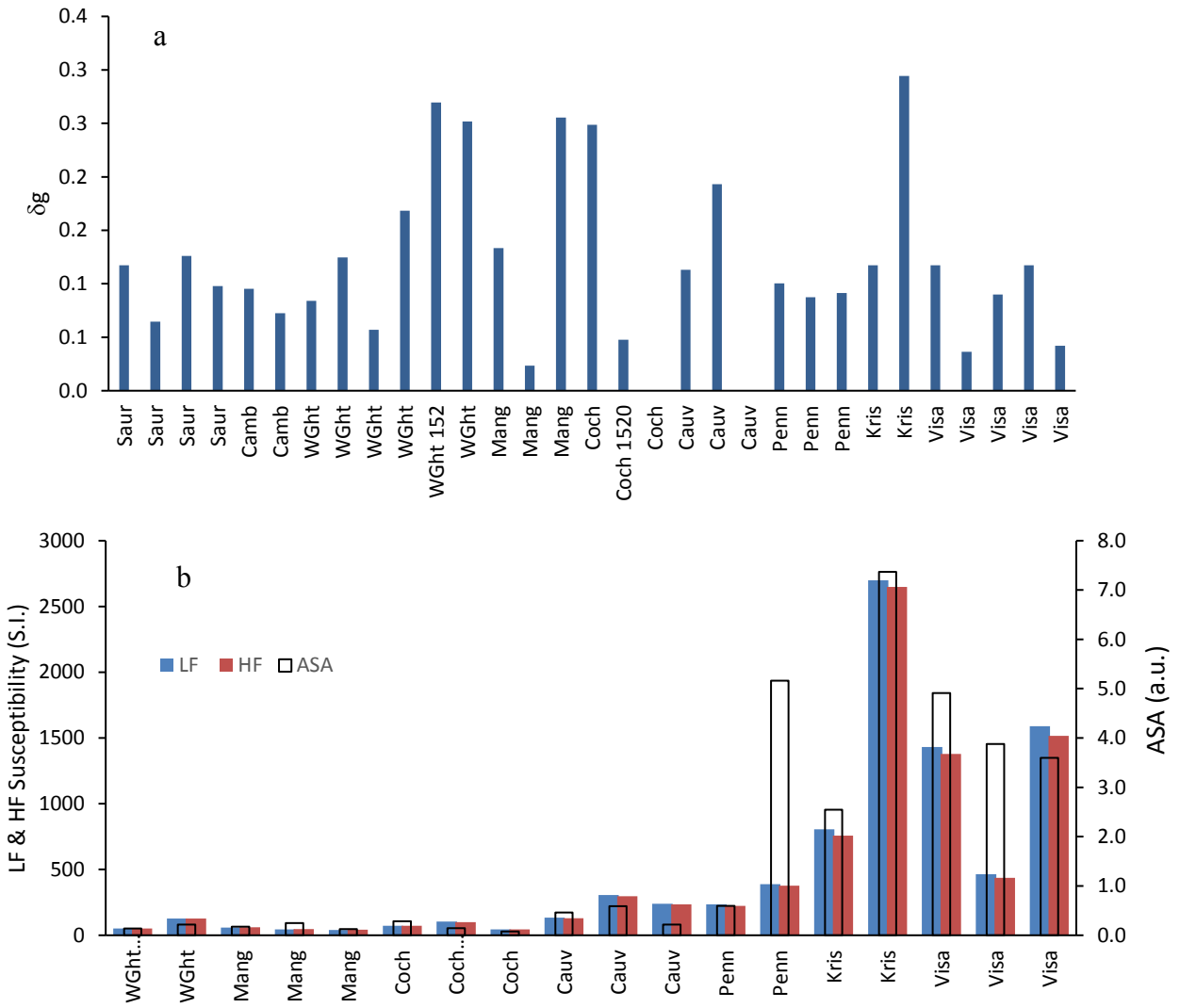
Fig. 6: The geographical variation in a) δg determined by spectral crossover field, b) correlation between LF, HF and ASA (open bars).

Table 2 EPR, metal and susceptibility Pearson correlation coefficient are for stations from the WC southerly Western Ghats stations to the EC N. Visakhapatnam deltaic stations.

	HF	ASA	PtP	*dH(T)*	Fe	Cr	Cu	Ni	Totl. Metals
LF	0.999	0.858	0.634	-0.279	0.792	0.821	0.821	0.738	0.792

5 Concluding remarks

We have demonstrated that EPR can be employed to evaluate the concentration and chemical form of paramagnetic metals in sediments from marine (and by extension, terrestrial) environments to yield distinctive EPR spectral 'fingerprints'; spectra that can be characterised quantitatively by employing an appropriate and detailed electromagnetic EPR model. Further, we have presented an EPR baseline study of metal ion concentrations in Indian continental shelf marine sediments impacted by anthropogenic pollution. The results indicate that there is considerable variation in the form and detail of the EPR spectra from along the continental shelf, the components of which reflect the coastal location and the origin of fluvial inputs. These in turn strongly contribute to the assemblage of paramagnetic species within the sediments. This bestows an EPR spectral 'fingerprint' upon the sediment, one that is sensitive to, and indicative of both location and inputs and, inversely, has the potential to assist in source apportionment in sediment un-mixing models and environmental impact assessment. As the EPR spectrum of many paramagnetic metal ions is unique and oxidation state dependent, constituent paramagnetically active metals can also be identified. In addition, g-values, g-shifts and hyperfine splittings, provide information on the (magnetic) micro-environment of metals within sediments. Chemical evidence has also been presented for bio-toxic concentrations of metals of anthropogenic origin impacting well beyond the shallow coastal margin. The progressive and distinctive largescale variation observed in the composition of the continental shelf sediments across the coastal sites is consistent with low lateral sediment transport as suggested by Borole (1988). The experimental methodology, results and analysis presented demonstrate that electromagnetic EPR spectroscopic modelling combined with AAS / ICP and environmental magnetism measurements are effective tools for the qualitative and quantitative analysis of marine environmental sediments.

Dedication

We dedicate this paper to the memory of Sambasiva Rao, Department of Chemistry, Pondicherry University, India, mentor and colleague and inspiration for this work.

Appendix A. Supplementary data

Supplementary data to this article can be found online at http://dx.doi.org/10.1016/j.scitotenv.2017.08.065

References

Abragam, A., Bleaney, B., 1970. Electron Paramagnetic Resonance of Transition Ions. Clarendon, Oxford.

Alagarsamy, R., 2006. Distribution and seasonal variation of trace metals in surface sediments of the Mandovi estuary, west coast of India, Estuarine, Coastal and Shelf Science 67, 333-339. doi:10.1016/j.ecss.2005.11.023

Alagarsamy, R., 2009. Environmental magnetism and application in the continental shelf sediments of India. Marine Environmental Research, 68, 49-58. doi: 10.1016/j.marenvres.2009.04.003

Alagarsamy, R., Zhang, J., 2005. Comparative studies on trace metal geochemistry in Indian and Chinese rivers. Current Science 89, 299-309. http://www.currentscience.ac.in/Downloads/article_id_089_02_0299_0309_0.pdf

Alagarsamy, R., Zhang, J., 2010. Geochemical characterization of major and trace elements in the coastal sediments of India. Environmental Monitoring and Assessment, 161, 161−176, 2010. doi: 10.1007/s10661-008-0735-2.

Angino, E.E., Hathaway, R., Worman, J., 1971. Identification of manganese in water solutions by electron spin resonance, *in* Nonequilibrium systems in natural water chemistry: Advances in Chemistry, Ser. No. 106, 299-308. doi: 10.1021/ba-1971-0106.ch012

Bahain, J.J., Falguères, C., Voinchet, P., Duval, M., Dolo, J.M., Despriée, J., Garcia, T., Tissoux, H., 2007. Electron spin resonance (ESR) dating of some European late lower Pleistocene sites, Quaternaire, Volume 18, 175-185. doi: 10.4000/quaternaire.1048

Borole, D.V., 1988. Clay sediment accumulation rates on the monsoon-dominated western continental shelf and slope region of India, Marine Geology, 82, 285-291. doi.: 10.1016/0025-3227(88)90148-X

Billon, G., Ouddane, B., Laureyns, J., Boughriet, A., 2003. Analytical and Thermodynamic Approaches to the Mineralogical and Compositional Studies on Anoxic Sediments. J Soils Sediments, 3, 180-187. doi: 10.1065/jss2003.04.074

Boughriet, A., Ouddane, B., Wartel, M., 1992. Electron spin resonance investigations of Mn compounds and free radicals in particles from the Seine river and its estuary. Marine Chemistry, 37, 149-169. doi: 10.1016/0304-4203(92)90075-l

Crook, N.P., Hoon, S.R., Taylor K.G., Perry, C.T., 2002. Electron Spin Resonance as a high sensitivity technique for environmental magnetism: determination of contamination in carbonate sediments, Geophysical J. International, 149, 328-337. doi: 10.1046/j.1365-246x.2002.01647.x

Deorukhakar, S.V., 2003. Arsenic in the coastal marine environment of India. Ph.D. Thesis, University of Mumbai, 1-146

Engin B., Kapan-Yeşilyurt S., Taner G., Demirtaş H., Eken M. 2006. ESR dating of Soma (Manisa, West Anatolia – Turkey) fossil gastropod shells, Nuclear Instruments and Methods in Physics Research B 243, 397–406. doi:10.1016/j.nimb.2005.09.008

Espinosa, M., Campero, A., Salcedo, R., 2001. Electron spin resonance and electronic structure of vanadyl-porphyrin in heavy crude oils, Inorg. Chem. 40, 4543–4549. doi: 10.1021/ic000160b

Gao L., Yin G.M., Liu CR , Bahain J.J., Lin M., Li J.P., 2009. Natural sunlight bleaching of the ESR titanium center in quartz, Radiation Measurements 44 (2009) 501–504. doi:10.1016/j.radmeas.2009.03.033

Guedes, C.L.B., Di Mauro, E., Antunes, V., Mangrich, A.S., 2003. Photochemical weathering study of Brazilian petroleum by EPR spectroscopy. Marine Chemistry, 84, 105-112. doi: 10.1016/s0304-4203(03)00114-2

Guilbault, G.G., Misel, T., 1969. Determination of mixtures of copper(II) and manganese(II) by electron spin resonance. Analytical Chemistry, 41, 1100- 1103. doi: 10.1021/ac60277a034

Guilbault, G.G., Misel, T., 1970. Some selective determinations of iron group elements in the presence of each other by electron spin resonance methods: Analytica Chimica Acta, 50, 151-156. doi: 10.1016/s0003-2670(00)80936-8

Guilbault, G.G., Moyer, E.S., 1970. The separation and determination of molybdenum by electron paramagnetic resonance. Analytical Letters, 3, 563- 571. doi: 10.1080/00032717008058582

Heise, J.J., 1968. Application of electron spin resonance spectroscopy to oceanographic samples. Marine Sciences Instrumentation, 4, 25 - 35.

Kersten, M., Smedes, F., 2002. Normalization procedures for sediment contaminants in spatial and temporal trend monitoring, J. Environ. Monit., 4, 109-115. doi: 10.1039/B108102K

Krishnan, M.S., 1968. Geology of India and Burma, Higginbothoms Ltd, Madras, p. 536. Permalink: http://www.worldcat.org/oclc/946052888

Küçükuysal C., Engin B., Türkmenoğlu AG., Aydaş C., 2011. ESR dating of calcrete nodules from Bala, Ankara (Turkey): preliminary results. Applied Radiation Isotopes 69(2): 492-499. Epub 2010 Oct 16. doi: 10.1016/j.apradiso.2010.10.005

Long, E.R., MacDonald D.D., Smith S.L., Calder F.D., 1995. Trace metal concentration for biological effects; from - Incidence of Adverse Biological Effects Within Ranges of Chemical Concentration in Marine and Estuarine Sediments, Environmental Management, 1995. doi: 10.1007/BF02472006

Mangrich, A.S. Da Silva, L., Pereira, B.F., Messerschmidt, I., 2009. Proposal of an EPR based method for pollution level monitoring in mangrove sediments, Journal of the Brazilian Chemical Society, Volume 20, 294-298, ISSN: 01035053

Manjunatha, M.P., 1992. A note on the factors controlling the sedimentation rate along the western continental shelf of India, Marine Geology 104, 219-224. doi: 10.1016/0025-3227(92)90097-2

Nagashima K., Asahara Y., Takeuchi F., Harada N., Toyoda S., Tada R., 2012. Contribution of detrital materials from the Yukon River to the continental shelf sediments of the Bering Sea based on the electron spin resonance signal intensity and crystallinity of quartz, Deep-Sea Research II, 61-64, 145–154. doi:10.1016/j.dsr2.2011.12.001

Otamendi A.M., Diaz M., Costanzo-Alvarez V., Aldana M., Pilloud A., 2006. EPR stratigraphy applied to the study of two marine sedimentary sections in southwestern Venezuela, Physics of the Earth and Planetary Interiors 154 243–254. doi: 10.1016/j.pepi.2005.04.015

Ouddane, B., Boust, D., Martin, E., Fischer, J.C., Wartel, M., 2001. The Post-Depositional Reactivity of Iron and Manganese in the Sediments of a Macrotidal Estuarine System. Estuaries, 24,1015-1028. doi: 10.2307/1353014

Pandarinath, K., Verma, S.P., Yadava, M.G. 2004. Dating of Sediment Layers and Sediment Accumulation Studies along the Western Continental Margin of India: A Review, International Geology Review 46, 939-956. doi: 10.2747/0020-6814.46.10.939

Rao, Ch.M., 1985. Distribution of suspended particulate matter in the waters of eastern continental margin of India. Deep-sea research. Pt.B 32, 12-16. doi: 10.1016/0198-0254(85)93741-0

Rao, K.L., 1975. India's water wealth, Orient Longman, New Delhi, 255 pp.

Rao, V.P., 1991. Clay mineral distribution in the continental shelf and slope off Saurashtra, west coast of India. Indian Journal of Marine Sciences 20, 1-6. http://nopr.niscair.res.in/handle/123456789/38169

Rao, V.P., Rao, B.R., 1995. Provenance and distribution of clay minerals in the sediments of the western continental shelf and slope of India. Continental Shelf Research 15, 1757-1771. doi: 10.1016/0278-4343(94)00092-2

Sangode, S.J., Sinha, R., Phartiyal, B., Chauhan, O.S., Mazari, R.K., Bagati, T.N., Suresh, N., Mishra, S., Kumar, R., Bhattacharjee, P., 2007. Environmental magnetic studies on some Quaternary sediments of varied depositional settings in the Indian sub-continent. Quaternary International, 159, 102-118. doi: 10.1016/j.quaint.2006.08.015

Sun, Y., Tada, R., Chen, J., Liu, Q.S., Shin, T., Tani, A., Ji, J., and Yuko, I., 2008. Tracing the provenance of fine-grained dust deposited on the central Chinese Loess Plateau: Geophysical Research Letters, v. 35, L01804. doi: 10.1029/2007GL031672

Tissoux, H., Toyoda, S., Falguères, C., Voinchet, P., Takada, M., Bahain, J.J., Despriée, J., 2008. ESR dating of sedimentary quartz from two pleistocene deposits using Al and Ti-centers, Geochronometria, 30, 23-31. doi: 10.2478/v10003-008-0004-y

Violante, A., Cozzolino, V., Perelomov, L., Caporale, A.G., Pigna, M., 2010. Mobility and bioavailability of heavy metals and metalloids in soil environments, Journal of Soil Science and Plant Nutrition, 10, 268 – 292. doi: 10.4067/s0718-95162010000100005

Virmani, Y.P., Zeller, E.J., 1974. Analysis of background copper concentrations in sea water by electron spin resonance. Analytical Chemistry, 46, 324-325. doi: 10.1021/ac60338a007

Wakeman, S., Carpenter, R., 1974. Electron spin resonance spectra of marine and fresh-water manganese nodules Chemical Geology, 13, 39-47. doi: 10.1016/0009-2541(74)90047-3

Supporting Information (Alagarsamy and Hoon)
Appendix 1

SI.1. Metals Analysis by ICPAS

For metal analysis a known mass (c. 0.2g) was digested in a mixture of concentrated HF–HNO3–HClO4 (Zhang and Liu, 2002). Solutions were analysed for the magnetically active metals Fe, Cr, Cu and Ni using an ICP-AES (Model: PE-2000). The accuracy of the analytical methods was monitored by analysing standard reference materials (GSD-9) with a study sample in every analytical batch. Further checks were made through repeated analyses of standard reference materials. Analytical precision was checked by triplicate analysis of standard materials with coefficients of variation found to be within ± 1-8% for each element.

SI.2. EPR Modelling

Sediment EPR spectra have been modeled electromagnetically from first principles by inputting spectra into a graphical user interface package developed at MMU, UK. This enables the relative contribution from constituent components to be fitted and determined generating an EPR 'fingerprint'. This reductionist approach is more subtle and distinctive than using bulk environmental magnetism parameters alone. EPR spectrometer settings and the susceptibilities and concentrations of principal magnetic components, comprise optimisable input (and consequently 'fingerprint') parameters into the electromagnetic model. To characterise EPR spectra quantitatively in this manner it is necessary to model the RF magnetic field dependent susceptibility, χ, in the presence of DC fields and solve the equations of motion of the magnetisation M precessing in the local effective field H. The model uses solutions to the electromagnetic Bloom-Block, Landau-Lifshitz and Kittel equations (Soohoo, 1985) to determine the EPR susceptibility in the low RF power levels that pervading the spectrometer cavity. The Bloch equation describes the motion of the transverse magnetisation, M_z, as

$$\frac{dM_z}{dt} = \gamma(\boldsymbol{M} \times \boldsymbol{H})_z - \frac{M_z - M_0}{\tau_1} \qquad (1)$$

where $\gamma = 2\pi g \mu_B / h$ is the electronic gyromagnetic ratio. The nature of the magnetic impurities and particles in the sediment determine, the spin-lattice relaxation time τ_1, and M_0, the component of the magnetisation parallel to the applied field. When a ferrimagnetic component is present, as

is often the case in environmental samples, magnetocrystalline and shape anisotropy need to be included as this alters the effective field experienced by the magnetic impurity. In EPR the magnetisation precesses around the local effective field, H_{eff}, rather than simply the spectrometer field, H. This results in the resonance condition,

$$f_0 = \frac{1}{2\pi}\gamma\mu_0 H_{eff} = g\mu_B\mu_0\, H_{eff}/h \qquad (2)$$

The Poynting vector $\boldsymbol{S}$ describes the RF power, P, absorbed by the precessing magnetisation due to positively and negatively circulating RF fields in the spectrometer cavity. Only positively circulating fields are experimentally significant. Thus P can be written as,

$$P = \mu_0\boldsymbol{h}_\perp \cdot \frac{d\boldsymbol{M}}{dt} = 2\pi\mu_0 f(\chi''_+ h_+^2) \qquad (3)$$

where χ''_+ is the EPR susceptibility responding to the RF field h_+. The EPR model thus requires and permits the input of spectrometer operating conditions and the optimisation of sample parameters. Spectrometer parameters include the microwave RF frequency (*c*. 9.5 GHz) and resonant cavity field (Am^{-1}) generated by the (*c*. 0.3 mW) microwave power in the high Q cavity. For each identifiable component in an EPR spectrum, the g-factor, volume fraction, dimensionless RF magnetic susceptibility, spin-lattice relaxation time τ_1 (nS) etc. are optimised to achieve the best fit between the experimental and modelled spectrum. If hyperfine splitting is present then the number (n≥1) of hyperfine peaks and their splitting field is also optimised. For ferrimagnetic components the saturation magnetisation (M$_s$ kAm^{-1}), uniaxial anisotropy constant (K Jm^{-3}) and FMR damping constant (α>0) are optimised. Field dependent ferrimagnetic particulate magnetisation is modelled using a Langevin parameter X defined by $M = M_s L(H \cdot X)$ where L is the anhysteretic Langevin function. The parameter X controls both low and high field ferrimagnetic susceptibilities and models magnetic fine particle systems very well (Hoon and Lambrick 2005). Line broadening due to magnetostatic interactions, can also be modelled using a number, *n*, of slightly field-displaced resonances and setting τ_1 to be sufficiently short such that the linewidths overlap. The model also allows a net demagnetisation factor to be selected ($0 \leq N \leq 1$) enabling the effect of sample geometry upon the local (demagnetising) field to be included. For dilute environmental samples, however, sample shape effects can usually be ignored. The model outputs the computed field dependent EPR absorption curve (differential and integral) along with those of each resolvable magnetic component, determined on the basis of materially relevant sample characteristics.

SI.3. Supporting References

Hoon S.R, Lambrick, D.B., 2005. Parametric modelling of magnetic fine particle systems: the role of single domain particle size distributions and magnetic anisotropy. Journal of Physics: Conference Series 17, 1–6. doi:10.1088/1742-6596/17/1/001

Soohoo RF, 1985. Microwave magnetics, New York, Harper and Row

Zhang, J., and Liu, C. L., (2002). Riverine composition and estuarine chemistry of particulate metals in China — Weathering features, anthropogenic impact and chemical fluxes. Estuarine, Coastal and Shelf Science, 54, 1051–1070. doi:10.1006/ecss.2001.0879.

SI.4. Supporting Figures
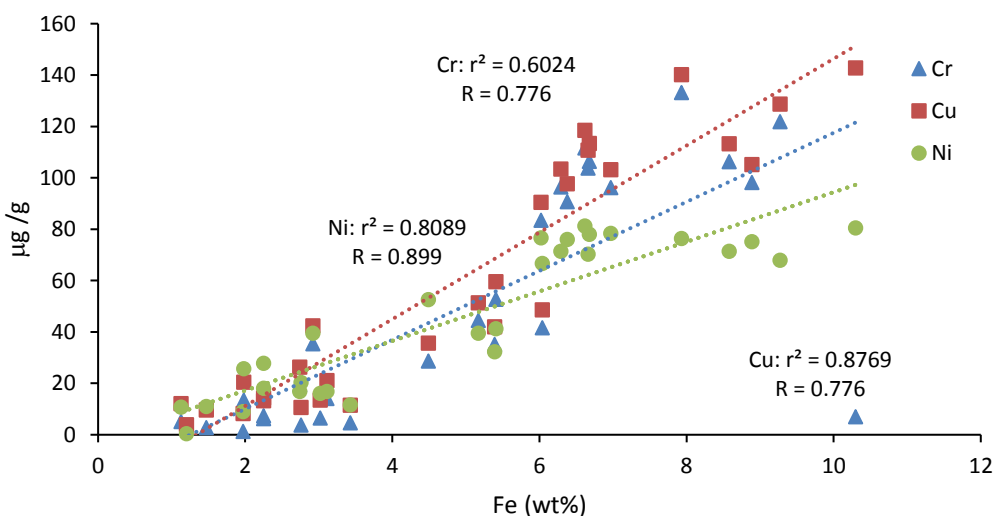
Fig. S1: Residual error r^2 and Pearson correlation Coefficients R for Cr (triangles), Cu (squares) and Ni (circles) versus Fe concentration.

Fig. S2: PtP (a.u.) versus total EPR absorption spectral area, ASA, (a.u.) between 0 and 0.5T.

Fig. S3: Total EPR absorption spectral area, ASA (a.u) vs total metal content (wt%).

Fig. S4: Shows clustering of peak width $\mu_0 dH$ around two principal values, when classified by total concentration of Ni, Co, Cu µg/g. The four outliers correspond to N Cochin and Cauvery stations.

SI.5. Supporting Tables

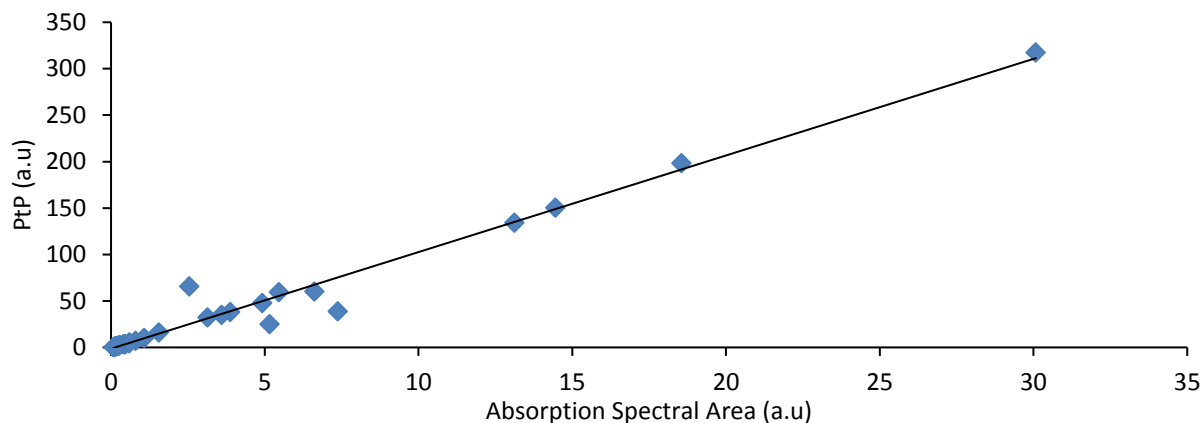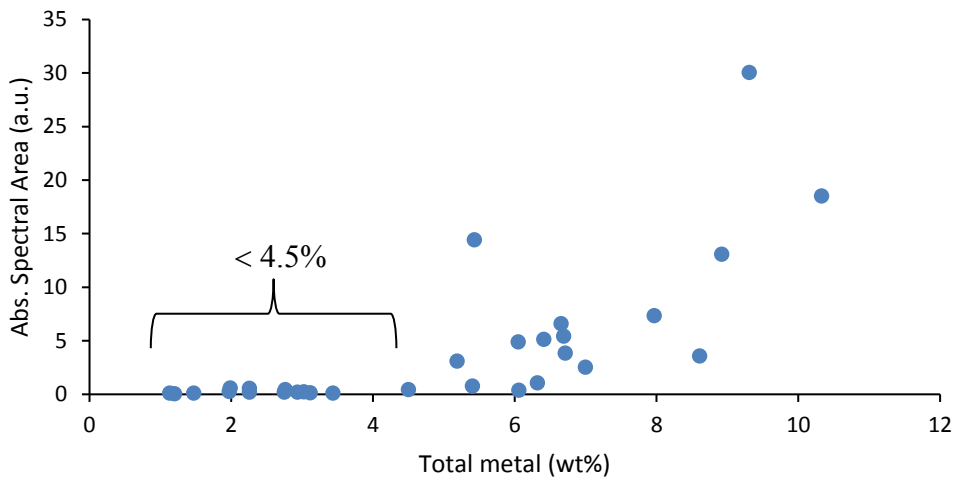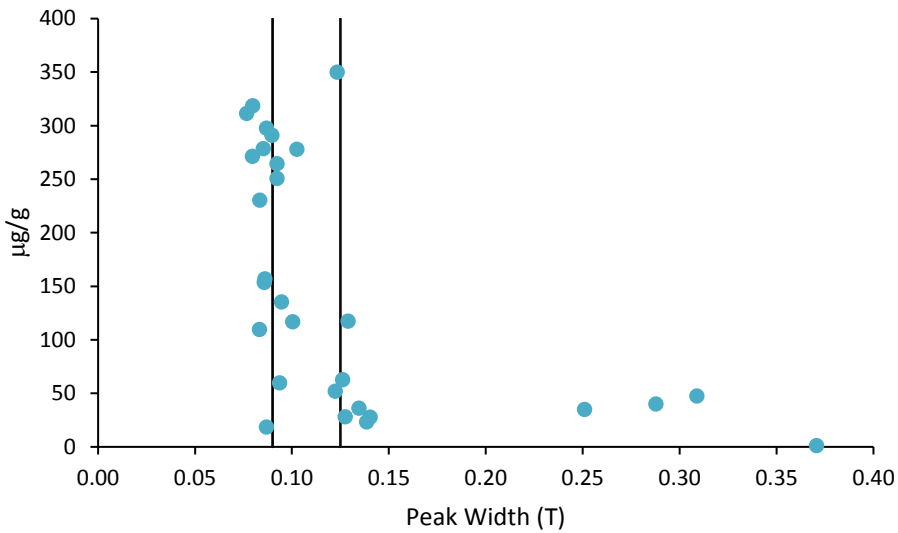Table S1: Sampling stations area, position, and dominant sediment. The four digit station ID shown geographically on Fig.1. Chronologically i) EC voyage 130, N to S, Jan, post Monsoon, ii) WC voyage 139, S to N, May/Jun., pre-Monsoon, iii) EC voyage 143, N to S, Nov., post Monsoon, iv) WC voyage 151, N to S, Mar, pre-Monsoon.

Voyage	N-S-E Rank	Station	Coastal Area	Dominant Natural Sediment.	Lat	Long	Depth (m)
130	34	3010	N Visa. delta.	Basaltic	$16^0\,26.0'$	$81^0\,31.0'$	40
130	33	3012	N Visa. delta.	Basaltic	$16^0\,26.0'$	$81^0\,31.0'$	40
130	32	3013	N Visa. delta	Basaltic	$16^0\,11.0'$	$81^0\,47.5'$	55
130	28	3014	Krishna	Basaltic	$15^0\,54.5'$	$81^0\,14.6'$	50
130	27	3017	Krishna	Basaltic	$15^0\,39.5'$	$81^0\,00.0'$	48
130	26	3019	N Penner	Basaltic	$15^0\,00.3'$	$80^0\,16.7'$	52
130	23	3024	N Penner	Basaltic	$12^0\,00.0'$	$80^0\,05.6'$	49
130	22	3025	N Cauvery delta	Basaltic	$12^0\,00.0'$	$80^0\,04.2'$	50
130	21	3026	N Cauvery delta	Basaltic	$11^0\,00.0'$	$80^0\,02.5'$	52
139	20	3164	N Cochin	Granite / Gneiss	$10^0\,02.5'$	$76^0\,00.0'$	35
139	19	3165	N Cochin	Granite / Gneiss	$10^0\,01.0'$	$75^0\,40.1'$	90
139	18	3171	N Cochin	Granite / Gneiss	$10^0\,58.2'$	$75^0\,39.0'$	33
139	17	3170	N Cochin	Granite / Gneiss	$10^0\,58.2'$	$75^0\,18.7'$	73
139	16	3173	Mangalore	Granite / Gneiss	$12^0\,00.0'$	$74^0\,40.0'$	75
139	15	3180	Mangalore	Granite / Gneiss	$12^0\,59.0'$	$74^0\,20.9'$	60
139	14	3182	Bhatkal	Granite / Gneiss	$14^0\,00.0'$	$74^0\,19.0'$	40

139	12	3191	SW Ghats	Granite / Gneiss	$14^0\,59.7'$	$73^0\,20.0'$	75
139	13	3192	SW Ghats	Granite / Gneiss	$14^0\,59.6'$	$73^0\,40.0'$	49
143	31	3242	Visa. delta	Basaltic	$16^0\,31.0'$	$82^0\,30.7'$	700
143	30	3244	S Visa. delta	Basaltic	$15^0\,39.1'$	$81^0\,06.4'$	660
143	29	3245	S Visa. delta	Basaltic	$14^0\,54.1'$	$80^0\,20.5'$	80
143	25	3248	Penner	Basaltic	$13^0\,30.5'$	$80^0\,31.7'$	120
143	24	3249	Penner	Basaltic	$13^0\,07.8'$	$80^0\,32.6'$	120
151	1	3440	N Saura. B	Basaltic	$22^0\,53.7'$	$68^0\,22.0'$	23
151	2	3441	N Saura. B	Basaltic	$22^0\,24.0'$	$68^0\,38.0'$	22
151	3	3443	S Saura. B	Basaltic	$21^0\,54.1'$	$68^0\,56.0'$	45
151	4	3444	S Saura. B	Basaltic	$21^0\,30.0'$	$69^0\,10.0'$	57
151	6	3452	N Gulf of Cambay	Basaltic	$20^0\,14.1'$	$72^0\,11.9'$	30
151	7	3453	S Gulf of Cambay	Basaltic	$19^0\,30.0'$	$72^0\,16.0'$	30
151	8	3462	Mumbai / NW Ghats	Basaltic	$18^0\,20.4'$	$72^0\,41.6'$	25
151	9	3463	Mumbai / NW Ghats	Basaltic	$17^0\,50.0'$	$72^0\,46.0'$	32
151	10	3464	W Ghats	Basaltic	$17^0\,19.0'$	$72^0\,50.0'$	60
151	11	3471	Mid W Ghats	Basaltic	$16^0\,06.0'$	$73^0\,00.0'$	70

Table S2: Sampling stations, depths and Fe, Cr, Cu and Ni concentrations.

The four digit station numbers are cross referenced geographically on Fig.1, not available (n.a.),

not detected (n.d.).

Part a

Voyage	N-S-E Rank Index	Station ID	Depth (m)	Fe wt %	Cr ppm	Cu ppm	Ni ppm
130	34	3010	40	n.a.	n.a.	n.a.	n.a.
130	33	3012	40	8.58	106.28	113.20	71.38
130	32	3013	55	6.68	106.40	113.32	77.92
130	28	3014	50	7.93	133.22	140.14	76.39
130	27	3017	48	6.97	96.20	103.12	78.36
130	26	3019	52	6.38	90.71	97.63	75.96
130	23	3024	49	2.25	7.39	14.31	18.12
130	22	3025	50	2.25	6.26	13.18	27.79
130	21	3026	52	2.76	3.71	10.63	20.37
139	20	3164	35	1.20	-3.10	3.82	0.32
139	19	3165	90	3.43	4.59	11.51	11.54
139	18	3171	33	1.99	-1.43	5.49	6.49
139	17	3170	73	1.97	1.26	8.18	9.02
139	16	3173	75	1.47	2.71	9.63	10.95
139	15	3180	60	3.02	6.52	13.44	16.07
139	14	3182	40	3.11	14.08	21.00	16.88
139	12	3191	75	1.13	5.17	12.09	10.69
139	13	3192	49	2.74	19.39	26.31	16.85

Part b

Voyage	N-S-E Rank Index	Station ID	Depth (m)	Fe wt %	Cr ppm	Cu ppm	Ni ppm
143	31	3242	700	6.66	103.76	110.68	70.20
143	30	3244	660	6.62	111.60	118.52	81.18
143	29	3245	80	6.02	83.46	90.38	76.67
143	25	3248	120	1.98	13.50	20.42	25.61
143	24	3249	120	1.67	5.41	12.33	7.80
151	1	3440	23	4.49	28.67	35.59	52.60
151	2	3441	22	6.04	41.64	48.56	66.70
151	3	3443	45	5.17	44.42	51.34	39.43
151	4	3444	57	5.41	52.66	59.58	41.20
151	6	3452	30	9.27	121.80	128.72	67.87
151	7	3453	30	10.3	7.00	142.78	80.47
151	8	3462	25	8.89	98.17	105.09	75.17
151	9	3463	32	5.39	35.12	42.04	32.28
151	10	3464	60	6.29	96.43	103.35	71.35
151	11	3471	70	2.92	35.39	42.31	39.53

Table S3: High (HF) and Low Frequency (LF) magnetic volume susceptibility by coastal location along the more mid latitude sections of the western and eastern coast.

	Station in NW-S-NE order	Coastal Location	Mean LF (SI vol. susc.)	Mean HF (SI vol. susc.)
West Coast Pre-Monsoon Voyage 139	3191	W. Ghats	51.0	51.7
	3192	S.W. Ghats	127.0	126.3
	3184	Bhat.	33.3	35.0
	3182	Bhat./Mang.	59.3	61.7
	3180	Mangalore	44.2	46.8
	3173	Mangalore	40.8	43.5
	3171	Mangalore	20.8	21.0
	3170	N. Cochin	72.3	72.3
	3165	Cochin	103.5	99.7
	3164	N. Cochin	44.8	45.2
East Coast Post-Monsoon Voyage 130 & 143*	3026	N. Cauvery	134.8	129.3
	3025	N. Cauvery	305.3	297.1
	3024	N. Cauvery	239.8	234.6
	3249*	S. Penner	52.0	51.2
	3248*	Penner	233.8	223.6
	3019	N. Penner	388.5	376.0
	3018	Krishna	1722.0	1666.7
	3017	Krishna	806.7	757.6
	3014	Krishna	2699.2	2649.0
	3245	S. Visa.	1431.0	1379.5
	3013	Visa.	463.5	436.5
	3012	N. Visa.	1590.0	1516.2

[Supporting Information Ends]